Surface Science Reports 81 (2026) 100678

Contents lists available at ScienceDirect

Surface Science Reports

journal homepage: www.elsevier.com/locate/surfrep

Review Article

Recent endeavoring in biosurface and biointerface analysis with kinetic electrons and ions

Oscar Malvar [a,b], Giacomo Ceccone [a], Paulina Rakowska [a,c,d], Miran Mozetič [a,e], Teresa Pinheiro [a,f], Miguel Manso Silván [a,g,*]

[a] International Union for Vacuum Science, Technique and Applications, Avenue de La Renaissance 30, B-1000, Brussels, Belgium
[b] Instituto de Micro y Nanotecnología, IMN-CNM (CEI UAM+CSIC), Isaac Newton 8, Tres Cantos, E-28760, Madrid, Spain
[c] National Centre of Excellence in Mass Spectrometry Imaging, National Physical Laboratory, Hampton Road, Teddington, Middlesex, TW11 0LW, United Kingdom
[d] National Biofilms Innovation Centre, School of Biological Sciences, Highfield Campus, University of Southampton, Southampton, Hampshire, SO17 1BJ, United Kingdom
[e] Department of Surface Engineering, Jozef Stefan Institute, Jamova Cesta 39, 1000, Ljubljana, Slovenia
[f] Institute for Bioengineering and Biosciences and Associate Laboratory I4HB, Institute for Health and Bioeconomy and Departmento de Engenharia e Ciências Nucleares, Instituto Superior Técnico, Universidade de Lisboa, Av. Rovisco Pais 1, 1049-001, Lisboa, Portugal
[g] Departamento de Física Aplicada, Centro de Microanálisis de Materiales and Instituto de Ciencia de Materiales Nicolás Cabrera, Universidad Autónoma de Madrid, 28049, Madrid, Spain

ARTICLE INFO

Keywords:
Vacuum
Biointerface analysis
Ion spectromicroscopy
Nanomechanical mass spectroscopy
Electron microscopy
Photoelectron spectroscopy

ABSTRACT

Research in the field of biointerfaces is currently expanding because of continuous scientific demands stemming from different areas of biology and biomedicine. The most challenging questions require new technological advancements, often emerging from apparently distant disciplines, such as vacuum science and technology (VST). If living systems are characterized by their molecular diversity and scaled hierarchical structure, VST provides a palette of bioanalytical techniques designed to disentangle emerging complex biointerface structures. We review crucial developments in bioanalytical systems concentrating on those based on kinetic electrons and ions. Developments in these techniques are closing the vacuum gap between the conditions required for a sensitive analysis and the natural environment of the sample (near ambient pressure analysis). The biomedical field has been the focus of most of the reviewed developments, with an emphasis on recent research related to microbiological analysis. Additional examples from environmental applications, zoology or agriculture (among others) are also presented.

1. Introduction

Vacuum is generally conceived as a strong antagonist to life [1,2], but, paradoxically, synthetic vacuum is an allied technology allowing not only a better understanding of living systems but also the development of diverse solutions to overcome life threats [3]. Pressure is in fact a critical parameter used in astrobiology to determine exoplanets with potential for life viability [4]. The reduction in pressure is directly linked to the loss of water, the dominant molecule in media hosting life (water vapor saturates at about 3000 Pa at room temperature). Namely, if the pressure is above the saturated water vapor pressure, the evaporation is marginal and any attempt to decrease the pressure below this natural limit will cause gasification of water molecules. Thus, liquid water is incompatible with high-vacuum conditions, which are necessary for the proper operation of many detectors. In fact, water starts boiling as soon as the pressure level decreases below the water vapor saturated pressure and the boiling prevents the achievement of high-vacuum conditions. In round numbers, 1 g of liquid water will produce roughly 1 litter of water vapor at atmospheric pressure (10^5 Pa) and as much as 10 million cubic meters of vapor at the pressure of 10^{-5} Pa. No pump can remove such a huge volume of water vapor in a reasonable time. Table 1 reviews the defined and characteristic vacuum ranges critical for a general view of the topics covered in this work.

Water boils at 100 °C at atmospheric pressure. Decreasing the pressure causes a decrease in the boiling temperature. For example, water boils at a pressure of approximately 3000 Pa at room temperature, and about 600 Pa at 0 °C. Ice sublimates, and the vapor pressure is still as

* Corresponding author. Departamento de Física Aplicada, Centro de Microanálisis de Materiales and Instituto de Ciencia de Materiales Nicolás Cabrera, Universidad Autónoma de Madrid, 28049, Madrid, Spain.
E-mail address: miguel.manso@uam.es (M. Manso Silván).

https://doi.org/10.1016/j.surfrep.2026.100678
Received 1 August 2025; Received in revised form 6 February 2026; Accepted 8 February 2026
Available online 10 February 2026

List of Acronyms

Techniques covered by the present review

AP-MALDI Atmospheric pressure-matrix assisted laser desorption ionization
- APT Atom probe tomography
- ESI Electro-spray ionization
- FEL Free electron LASER
- HV high vacuum
- IBA Ion Beam Analysis
- IL ion induced luminescence
- IPEM Ion photon emission microscopy
- LV low vacuum
- MSI Mass spectroscopy imaging
- NMS Nanomechanical mass spectrometer
- PIF Proton induced Fluorescence
- PIXE Proton induced x-ray emission
- RBS Rutherford backscattering spectroscopy
- SEM Scanning electron microscopy

ESEM Environmental SEM
- SIMS Secondary ion mass spectrometry

CryoSIMS Cryogenic SIMS
OrbiSIMS Orbitrap analyzer SIMS
ToF-SIMS Time of flight SIMS
MeV-SIMS Megaelectronvolt SIMS
- STEM Scanning transmission electron microscopy

WetSTEM wet STEM
- STIM Scanning transmission ion microscopy

FSTIM Forward scattering STIM
- UHV ultra high vacuum
- XPS x-ray photoelectron spectroscopy

Cryo-XPS Cryogenic XPS
NAP-XPS Near ambient pressure XPS
APPES or APXPS Atmospheric pressure/ambient pressure XPS

large as 10^{-3} Pa at −100 °C. That's why cryogenic temperatures are needed if materials containing water are to be placed in ultra-high vacuum (UHV) chambers.

The saturated vapor pressure of water at the temperature of liquid nitrogen (approximately −200 °C) is below 10^{-20} Pa, that is, negligible. This is the general thermodynamic framework for cryopreservation, which is valid if the probing techniques do not harm the sample configuration. Thus, cryogenic methods have been successfully developed and used for decades within vacuum systems to study native biological structures in parallel to resin embedding or chemical staining methods [5–10].

Many examples of vacuum-related technological developments demonstrate that this is by no means a declaration of total incompatibility between vacuum and life. There are two main reasons for this: a) Life is a cyclic process, so vacuum can be present in a latent state of life and subsequently bloom under more favorable wet conditions, which leaves the debate open with respect to the origin of life. b) Water binds to biomolecules and bioinorganic structures at extremely different degrees of interaction, so there is an increasing range of mild vacuum conditions (close to water vapor saturated pressure) in which biological systems can be studied in close to functional states.

Since the efforts of Castner et al. [11] and Kasemo [12] to integrate different methods that scientists have used for the characterization of biological surfaces and interfaces, many achievements have been made in the area of biointerface characterization. In this review, we highlight recent developments emerging from the application of different vacuum technologies to increase our knowledge of biomolecular interfaces. We highlight here that the object of study is rarely a whole living organism, but rather a section of it (a set of biomolecules for instance), which may require stringent sample preparation procedures to keep its natural structure in compatibility with measurement conditions. Most of the techniques discussed in this paper are used to characterize biological materials including biomolecules (proteins, nucleic acid, lipids, carbohydrates …) with increasing complexity up to cells and tissue.

The use of vacuum-related characterization techniques to decipher the structure of biointerfaces is described in the first section. Contributions from spectroscopies relying on kinetic particles (defined as accelerated ions free of a hosting condensed matter phase independently of their elemental or molecular nature) are covered, highlighting the specific requirements for appropriate sample preparation. In the second section, we introduce new nanomechanics-based mass spectrometers, which increase the range of detectable masses for biological structures, allowing the detection of single-virus or even single-bacteria samples. The following section is devoted to ion beam analysis (IBA) techniques, and their projection in the biointerfaces field. The fourth section describes advances in systems that allow spectroscopy or microscopy (or both) to be performed on biological systems at increasingly high pressures ("near ambient pressure", "environmental" or even "atmospheric pressure"). In fact, the progress of biointerface analysis is taking place in parallel with the development of new instrumentation to make the classical electron and ion analytical techniques compatible with new environmental conditions. The approaches are reviewed in Table 2. This progress is essential to characterize biological structures restricting the loss of bio-structural water, whether by cryogenic procedures or by maintaining sample in a pressure range from ambient, to 100 Pa since at this pressure and room temperature there is still a strong bonding of water molecules to fundamental biological structures such as proteins. Loosely bound water may eventually be evacuated by the vacuum system (LV limit).

The fact that biological samples contain water with different degrees of cohesion implies a risk of a denaturing process because of water loss via vacuum exposure (especially in UHV chambers). This phenomenon takes place even at low cryogenic temperatures in the first vacuum cycles, prior to exposure to any kind of radiation. For instance, though cryo-X-ray photoelectron spectroscopy (Cryo-XPS, XPS is widely used in biomedical surface analysis [25,26]) has been employed to characterize several biological species such as bacteria, microalgae and viruses [27], there has been a latent ambition to carry out analyses at pressures closer to the natural environment. A lot of progress has been made, and processes to circumvent dehydration, such as the use of capsules with electron transparent membranes, have been developed. Although sample preparation is not always fully satisfactory, the capsule pressure is high, as is the relative vapor pressure of water, which contributes to preserving the natural structure of biological matter. An alternative to

Table 1
The vacuum ranges as defined in the international union for vacuum science technique and applications.

Vacuum Level	Atmospheric Pressure (AP)	Low Vacuum (LV)	Medium Vacuum (MV)	High Vacuum (UHV)	Ultra High Vacuum (UHV)	Extreme High Vacuum (EHV)	Interplanetary Pressure
Pressure (Pa)	10^{5}	$<10^{5}$-10^{2}	$<10^{2}$-10^{-1}	$<10^{-1}$-10^{-6}	$<10^{-6}$-10^{-9}	$<10^{-9}$	$<10^{-8}$-10^{-14}

Table 2
Alternatives for the microscopic and spectroscopic analysis using kinetic ions or electrons for biological samples with caution for preservation of natural structure by cryogenic or sample environment approaches.

Pumping	Conventional	Conventional	Differential	Not required for sample stage
Sample holder	With cryo cooling	Electron/ion transparent graphene or SiN membrane capsule	Conventional (with or without cooling)	Conventional, mildly cooled, vented
Sample pressure (Pa)	$\sim 10^{-5}$	$\sim 10^{-5}$	$\sim 10^{2}$-10^{3}	10^{5}
Techniques & Operation mode	XPS [13,14], SIMS [15], SEM [16], STEM [17],	SIMS [18], SEM [19], STEM [20]	NAP-XPS [21], ESEM [2], wetSTEM [22]	μPIXE [23], IPEM [24]
Challenges/ limitations	Sample preparation should avoid phase separation. Direct/indirect sample damage.	Sample exposure limited to potential capsule perforation. System damage by pressure jump.	Caution, direct/indirect sample damage.	Potential sample activation. Dosimetry. Limited spatial resolution.

those processes is the development of new instrumentation that makes the production and transport of electrons and ions in vacuum compatible with the preservation of biological samples under nearly atmospheric pressure conditions. Table 2 illustrates the most common ways available to perform electron microscopy or spectroscopy analysis of biological samples at nearly ambient pressure/close to atmospheric conditions. The table also reviews the main challenges from the point of view of sample preparation and required vacuum technology for the application of the techniques. The pressure gradient along a vacuum tube is governed by the ability of the vacuum pump to remove the gas, and by the flow with which the gas is introduced through an aperture. The gradient should be as large as possible to suppress scattering of electrons or ions on gaseous molecules. The volume flow, which is usually referred to as the "effective pumping speed" (i.e., the volume of gas removed in a unit time, the SI unit is m^3/s) at a given position in the vacuum tube, is:

$$S_{eff} = \left(1/S_{pump} + 1/C_{tube}\right)^{-1}$$

Here, S_{eff} is the effective pumping speed at a given position along the vacuum tube, S_{pump} is the pumping speed of the pump, and C_{tube} is the conductivity of the tube for the selected gas. The conductivity increases with increasing diameter of the tube and decreases with the length. When the conductivity is small compared to the pump's pumping speed (likely in practice), the effective pumping speed will be almost equal to the conductivity, so nearly independent of the pump. This means that the amount of gas removed from the tube (and thus the pressure gradient) cannot be increased by installing a more powerful pump. This natural limitation is overcome by differential pumping: the vacuum tube/circuit is segmented (differentiated) into several short portions, which are separated by apertures of small diameters. Each segment of the tube is pumped with a powerful pump, and the pump characteristics are selected according to the pressure level inside each segment. The vacuum tube between the chamber where a sample is positioned and the UHV chamber where the electron (or any other) detector is positioned is thus pumped with different pumps, so the gas removal is not governed by the properties of the pump used for pumping the detector, but rather by the properties of the pumps used for pumping each segment of the tube between the sample and the detector. Typically, the first segment from the sample is pumped by a rotary pump with the ultimate pressure below 1 Pa. The second segment is pumped with a high-vacuum pump, such as a turbomolecular pump, which ensures a tolerable gas flow into the chamber where the detector is located, typically within an ultra-high-vacuum chamber. Describing the engineering of these vacuum segments, sometimes in compatibility with enclosing systems to preserve the biological sample, is one of the main objectives of this review.

Pure water is rarely placed in a vacuum chamber. The boiling point of azeotropes (liquid mixtures that maintain equal molecular rates in gas and liquid phase) is generally different from that of a pure liquid, but not significantly, as compared to pure water.

Furthermore, water in biological tissues is encapsulated within cells, so matter such as seeds or even fruit can be kept in vacuum chambers where the pressure is well below the water vapor saturation pressure.

Some almost centenary techniques, such as transmission electron microscopy (TEM), have been used to characterize biological matter, having given rise to a whole set of sample preparation protocols and derived scientific results. The relevant structural information obtained is not in the scope of this review and readers may consider visiting reviews on the topic, which include recent research in-liquid cells or 3D structure analyses [7]. In the same way, the contributions from some emerging instruments, such as free electron lasers (FEL) and synchrotron sources are not considered as long as the means for the analyses are photons (photoelectrons derived from interactions from X-ray photons are considered). FELs working in the terahertz frequency range are opening new exciting opportunities in structural biology and biointerfaces via the "diffraction-before-destruction" effect [28,29]. This means that despite the highly energetic radiation used, the dosing in femtosecond pulses allows providing doses of giga Grays, essential for giving rise to identifiable diffraction patterns before the sample is pulverized. X-ray microscopies in synchrotron facilities (such as scanning transmission X-ray microscopy [30]) can analyze biological samples with unprecedented resolution in both 2D and 3D [31–38]. The deep penetration of X-rays and the recent developments in synchrotron radiation micro-X-ray fluorescence spectrometry, microtomography and dynamic micro-computed tomography allow studying the temporal evolution of samples [39,40]. To date, high-absorption contrast tomograms have been obtained for mineralized materials. However, it remains to be seen whether high-contrast images of organic materials can be obtained without the use of metal impregnation of tissues as contrast enhancers [41]. These breakthroughs remain also out of the scope of this work in view of the photonic nature of the analytical system.

The palette of techniques/processes described in this work to characterize biointerfaces should be complemented by the reader with other nonvacuum techniques working in environmental or even wet conditions. The properties determined through these techniques provide additional information on the specific biointerface system. Importantly, the functional inspection of such a biointerface system eventually requires contact with a wet medium. This may be as straightforward as immersion in a biomolecular buffer or as complex as implantation within a tissue/organ. For these tests, it is advised to consult a methodological bibliography related to molecular biology, microbiology, cell biology or tissue engineering [42–45].

For advanced in-line monitoring of biointerface functionality/performance, an active system of electrical, optical or miscellaneous nature should be used. The number of works related to in situ monitoring of biointerfaces is vast, but the basics of quartz crystal microbalance [46], surface plasmon resonance [47], vibrational sum frequency generation [48] and electrochemical analysis of biointerfaces are essential [49]. Notably, these techniques, which are not reviewed in this work, involve key structures engineered through vacuum processes. This instrumentation is considered a second-order contribution of VST to the field of

biointerfaces.

2. Biointerface analysis via mass spectroscopies and related bioimaging

The use of surface analysis for the assessment of the chemistry of biointerfaces started more than 40 years ago and was related mainly to the investigation of the surface properties of biomaterials [50–52]. In particular, much attention has been given to the characterization of surface modifications obtained with different techniques, such as low-temperature plasma processes [53–55], self-assembled monolayers [56], chemical reactions and biomimetic patterning [57], to improve and control medical device performance [58]. Furthermore, for the development of advanced biosensors, which require careful control of surface functionalities at the micron and submicron scales, the use of surface analysis techniques has been of paramount importance. In particular, time of flight secondary ion mass spectroscopy (ToF-SIMS) [59,60] has been extensively used to characterize protein and peptide-surface interactions at both the micro [61–64] and nano scale [65,66]. For example, ToF-SIMS has been used to address different challenges in biology and medicine with particular emphasis in imaging of cells and tissues [67]. Therefore, over the past two decades, progress in mass spectrometry and mass spectrometry imaging (MSI) has been driven by many biological applications [68]. Recent technical developments, such as cluster ion beams and DC beam technologies, have opened great opportunities in the use of ToF-SIMS in the biomedical field, increasing the possibility of performing 2D and 3D analyses beyond the static limit and reducing the image and spectral acquisition times [69–71]. The static limit is the maximum ion primary dose at which the integrity of the surface layer under analysis is maintained (static analysis conditions). Usually, a dose of 10^{13} cm^{-2} is considered as static limit. However, in case of samples sensitive to radiation damage a value of 10^{12} cm^{-2} is considered more appropriate. Typically, the mass range of a ToF-SIMS analyzer is from 0 to 10,000 amu (m/z) with a mass resolving power (mass resolution, M/DM) above 10,000 m/z. Some modern instruments can provide mass resolution above 15,000 m/z (e.g. J105 IonOptika, PHI NanoToF3+) or even up to 30,000 m/z (ionTOF M6).

Moreover, the introduction of atmospheric pressure matrix-assisted Laser desorption/ionization (AP-MALDI) [72] and the orbitrap analyzer SIMS (3D OrbiSIMS) [73,74] have led to new achievements. This analyzer provides ultimate spatial resolution of 50 nm (ionTOF hybridM6, https://www.iontof.com/) and very high mass resolving power (>240,000 @ m/z 200) resulting in a significantly improved confidence. The key advancement stems from the hybrid detection of the MS signal provided by an orthogonal ToF analyzer, with high in-depth and lateral resolution, and an orbitrap analyzer, with high mass resolution. The 3D imaging capabilities can be added by using primary ions from the liquid metal ion gun or gas cluster ion beam for profiling, as sketched in Fig. 1. The choice of optimal technology must be driven by a previous choice of the main scientific and technological interest, where high mass resolution in the spectra may prevent high spatial imaging resolution and vice versa. This may simply imply sequential acquisitions of data with particular equipment, but simultaneous high mass and high spatial resolution can be obtained with the J instruments from IonOptika [75], which is a significant advancement when demand of users for a system increases.

SIMS methods can provide label-free analysis in 3D. However, one of the major challenges in the application of SIMS to biological samples is the preservation of the sample's native, hydrated structure. As high-vacuum conditions (<10^{-8} Pa) are necessary to obtain high-quality SIMS data, biological samples must always be carefully dried before SIMS measurements. One of the first attempts to protect biointerfaces from dehydration was produced by using a trehalose (glucose disaccharide) protecting layer on proteins, which could be described in a closer to conformational state by ToF-SIMS when compared to

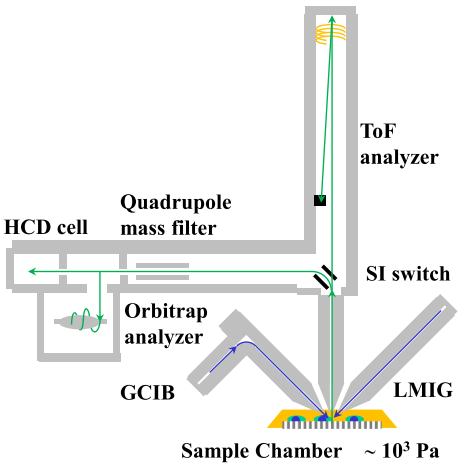

Fig. 1. Schematic representation of a commercially available orbiSIMS [73] system incorporating an orbitrap analyzer. Primary ions (whether from a gas cluster ion beam (GCIB) or from a liquid metal ion gun (LMIG)) impinge the sample and generate the secondary ions (SI), which can be analyzed twofold; by using a time of flight (ToF) analyzer for high surface-spatial resolution imaging or by using an orbitrap analyzer for high mass resolution. In this second mode, molecular fragments can be further analyzed in a higher energy collisional dissociation cell (HCD). Adapted from Ref. [73].

unprotected proteins [76]. This motivated MSI analysis of eukaryotic cells by using trehalose [77]. To quantitatively estimate the hydration protection capacity of trehalose, binding studies with streptavidin demonstrated more than 90% preservation of the original binding ability of a trehalose protected form after drying and rehydration [10]. The development and optimization of sample preparation protocols has been one of the major debate challenges in the SIMS community since early this century [78].

Several sample preparation protocols for in vacuo analysis, such as freeze-drying, resin embedding or histological fixation, are well established. However, these factors are known to influence sample morphology and can lead to delocalization of molecular signals and changes in chemical composition within samples, as well as loss of ultrastructural information and the appearance of artifacts [79–82]. These issues can be particularly severe in cases of high-spatial-resolution analysis, which is routine for NanoSIMS ion microprobes, where elemental imaging can be performed with a spatial resolution down to 50 nm, as can be achieved using advanced molecular imaging by time-of-flight ToF-SIMS instruments. Fig. 2 depicts the main functional components of the NanoSIMS and the working principle allowing both high mass and lateral resolution.

Cryo-SIMS has emerged as a solution to overcome sample degradation and derived analytical artifacts. Analysis of frozen-hydrated samples allows immobilization of water and prevents ultrastructural reorganization and the loss or translocation of water-soluble molecules, with the added advantage of samples being preserved in the closest form to the native state. The cryo-SIMS concept is not entirely new and has been demonstrated by early reports, where a cryogenic sample holder was used for the analysis of frozen-hydrated samples, prepared by cryo-fixation followed either by fracturing in vacuum or by direct transfer to the instrument [78,83,84]. Examples of identification of characteristic compounds, imaging modes and generation of 3D images from cells can be viewed in Fig. 3. These are nontrivial procedures, and it is difficult to control the conditions and products of the freeze-fracture process. With the advent of new high-spatial-resolution instruments, cryogenic preservation of high-finesse samples has become increasingly important, and novel solutions are starting to emerge. There are two equally important aspects to the progression of cryo-SIMS: the development of instrumentation and the development of advanced methods compatible with chemical imaging, cryo-preparation and handling [85,86]. All these

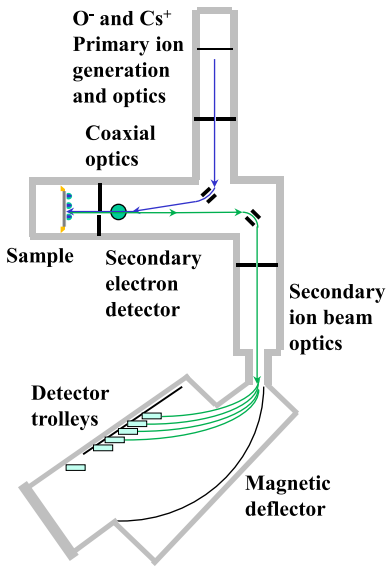

Fig. 2. Schematic representations of commercially available NanoSIMS system. Primary ions (O^- or Cs^+) are prepared (energy, current, collimation) in a vertical column and deflected to impinge the sample in the normal direction (in blue). Generated secondary ions are sent back using the same optics, along with secondary electrons, which are used for high resolution imaging. Secondary ions are driven to a magnetic sector, analyzed for high mass resolution and correlated with imaging data. Adapted from Ref. [73]. (For interpretation of the references to color in this figure legend, the reader is referred to the Web version of this article.)

contribute to validate the application of sample cryo-preservation protocols on new biological systems and, in case of frustrated validation, to the proposition of alternative protocols.

Cryogenic methods have been successfully developed and used for decades by the electron microscopy community to study native biological structures, and methods with no additives for embedding or staining (i.e. resins or osmium salts, respectively) have been adopted by other areas of analytical vacuum sciences [5–9]. A good example is the recently developed 3D OrbiSIMS instrument with cryo-capability, which allows seamless and straightforward transfer of cryogenically prepared samples without their exposure to atmospheric conditions into the vacuum and cryogenic temperatures of the SIMS instrument [15]. The instrument is equipped with a cold stage and a docking station compatible with a cryogenic sample transfer shuttle commonly used in electron microscopy.

Several other cryo-SIMS workflows for the introduction of cryogenic samples to SIMS instruments have been developed, including in-house-built and commercial solutions [88,89]. These factors provide better control over the cryogenic conditions of sample handling and analysis. However, cryo-SIMS is still far from a routine technique. Considerable effort is also needed to develop adequate sample preparation methods [90–92]. For example, plunge freezing is normally used for freezing cell samples for cryo-SIMS. However, it is not suitable for thicker biological samples, such as tissues or bacterial biofilms, as it can yield crystalline ice formation in samples thicker than 10 μm and cause sample damage because of insufficient cooling rates. High-pressure freezing works well for samples up to 200 μm thick. However, this technique often requires the addition of a cryoprotectant to the sample, a substance used to fill residual gaps between the sample and the sample carrier to prevent damage to the sample during freezing. There are tens of types of different cryoprotectants [93], and while they may be well suited for electron microscopy studies and generally for elemental NanoSIMS mapping, their chemistry can have detrimental effects on chemical and molecular SIMS analysis, leading to severe matrix effects and signal suppression, enhanced fragmentation or the presence of adducts.

Zhang et al. [15] surveyed different cryoprotectants for high-pressure freezing followed by cryo-SIMS analysis of mature bacterial biofilms. Among the tested cryoprotectants, the 150 mM ammonium formate solution was the most suitable. Each cryoprotectant could affect the chemistry of a high-pressure frozen sample. Therefore, this method should be chosen carefully, case by case, depending on the type of studied samples, analysis and desired results. Cryoprotectant approaches cannot be considered general and have consequently become an active field of research for bio sample analysis. However, with all the described methods the possibility of introducing artifacts that can lead to mistakes in data interpretation is quite easy.

Moreover, all these methods provide dead cells and tissue samples, while the possibility of using mass spectrometry imaging (MSI) techniques [94] on living biological systems has always been considered a

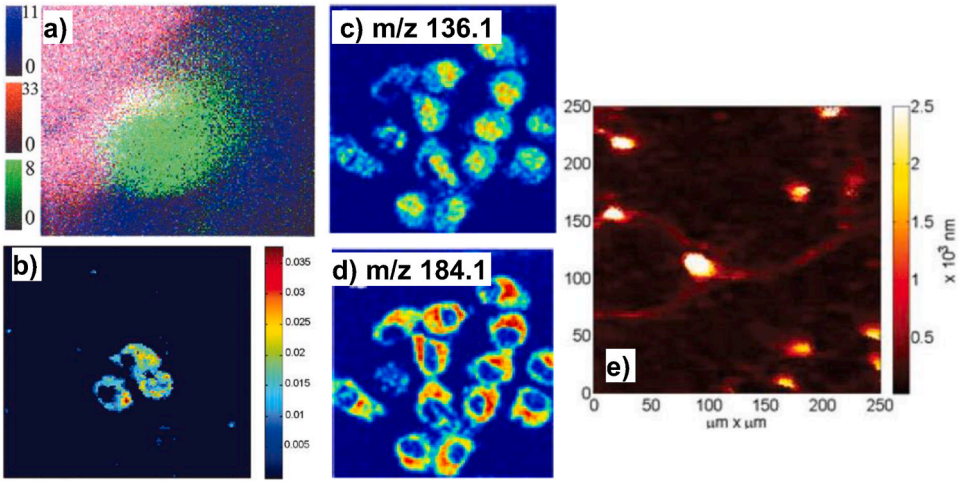

Fig. 3. Chemical imaging with samples prepared with optimized cryogenic processes. a) 100-μm-wide overlaid ToF-SIMS images of a phosphocholine/cholesterol liposome on a silicon wafer. See color intensity scales on the left; water channel in blue, silicon in red and C3 hydrocarbon in green [78]. b) 116 × 116 μm ToF SIMS image showing the distribution of the phosphocholine headgroup at *m/z* 184 in PC12 cells [83]. c and d) ToF SIMS images from Freeze fractured-frozen hydrated HeLa-M cells. The images are sections at identical stage revealing two different masses characteristic of the cytosol (adenine *m/z* 136.1, c) and the membrane (phosphocholine head group, *m/z* 184.1, d). Images are 250 μm wide. 3D mass spectral images available in Ref. [84]. e) Topographic imaging constructed from principal component analysis of the ToF-SIMS signatures of a neuronal cell network upon depth profiling and a scaling based on interferometry (see vertical scale) [87]. (For interpretation of the references to color in this figure legend, the reader is referred to the Web version of this article.)

'real' breakthrough. Contributions in this direction are discussed in section 5.

Synthetic interfaces, such as those prepared by plasma polymerization/modification processes, are additional objects of analysis by ToF-SIMS. Changes in surface properties shortly after plasma treatment can be detected by simple water contact angle measurements, where a decrease in wettability is usually observed (plasma can be employed to increase surface hydrophilicity via proton donor or proton acceptor groups [95] or to render surfaces superhydrophobic [96]). This method quickly provides information about surface changes and reveals the time scale in which the influence of plasma modification is the highest and in which further processing procedures should be conducted. Interestingly, these first signs of plasma aging are hardly detected by the change in chemical composition via XPS. The main reason is that the depth of XPS analysis is approximately 5–10 nm, and in this stage, functional groups are still present in the top surface layer. A more powerful tool for the detection of chemical aging is ToF SIMS, which can detect changes in the chemical composition of the first atomic layer [95,97,98].

Together with the growing popularity and advancements in SIMS and MSI techniques, a new branch of metrology will need to be approached before truly reliable measurements and analyses are created. It will soon become beneficial to establish a metrology framework aimed at interlaboratory comparisons, such as the Versailles Project on Advanced Materials and Standards (VAMAS), to guide fundamental studies and areas for further development. Furthermore, data storage, processing and analysis present additional emerging issues that can surely be approached by current emerging artificial intelligence tools. In fact, MSI can produce a large amount of data. Therefore, an increase in the storage capabilities of computers and further development of principal component analysis (PCA) and multivariate analysis (MVA) techniques, which are already routinely employed [87,99–103], should be made. An example providing global topographic imaging from interconnected neurons by using principal component analysis is available in Fig. 3e. The 101th IUVSTA workshop recently reviewed the current state of the art in the use of machine learning/artificial intelligence in the interpretation of SIMS data [104].

In addition to new developments in mass spectrometry, other related advanced techniques, such as atom probe tomography (APT), have yielded promising results when applied to studies of biointerfaces and organic materials. The sample preparation consists of a conical tip prepared with the sample material to provide a final radius of circa 50 nm. For inspection a high electric field induced under UHV ($\sim 10^{-8}$ Pa) is used to evaporate the atoms present on the conical tip structure. MS is used to analyze the sputtered atoms and the x-y coordinates of the sample, and with the time of detection one can detect depth of inspection, thus reproducing a 3D elemental map of the sample tip. For example, APT has been successfully employed to characterize bone mineralized tissue [105], proteins [106], and cells [107].

3. Nanomechanical mass spectrometry

As explained in the previous section, conventional mass spectrometry can identify biological molecules by measuring the mass−charge ratio with high sensitivity but is limited to light analytes [108,109].

In recent years, nanomechanical resonators have emerged as powerful tools for measuring the mass of intact biological entities with outstanding mass sensitivity [110] and a high dynamic range [110–113]. A nanomechanical resonator (like microcantilevers or double-clamped beams) holds natural frequencies that strongly depend on its mass and stiffness with given mode shapes [114]. The working principle is that its vibration is highly sensitive to its mass in such a way that when a particle is adsorbed on the resonator surface, its frequency decreases. Neglecting stiffness effects, the relative frequency downshift is proportional to the analyte mass and is given by Ref. [115]:

$$\frac{\Delta f_n}{f_n} = -\frac{1}{2}\frac{\Delta m}{m}\psi_n(x_0)^2$$

where Δf_n is the n^{th}-*mode* instantaneous downshift frequency upon particle adsorption, f_n is the n^{th}-*mode* frequency before the jump, m is the resonator mass, Δm is the particle mass, x_0 is the landing position and ψ_n is the n^{th}-*mode* shape. However, its behavior highly degrades when the resonator is immersed in a fluid (such as air or liquid) because of the decrease in the mechanical resonance quality factor, Q, which is defined as the ratio between the stored vibrational energy and the energy lost per cycle of oscillation. One way to overcome this limitation is to embed a microchannel inside a nanomechanical resonator, known as a suspended microchannel resonator (SMR) [116–118]. In these novel devices, biological entities flow in liquid through a microfluidic channel while the nanomechanical sensor is placed in HV, reducing the viscous drag, increasing its quality factor, and thereby increasing its mass sensitivity. Another method is the use of nanomechanical spectrometer systems (NMSs), where the analytes are transported from the liquid to the gas phase by means of soft ionization techniques and sent to the nanomechanical resonator surface, which is placed in a vacuum. In this section, we focus on nanomechanical spectrometry.

The first work related to NMS described above was published in 2002 by A. K. Naik et al. [119]. After this first publication, a series of new advancements were incorporated, such as the characterization of proteins by measuring two resonant modes [120] in real-time, the measurement of not only the mass but also the stiffness of bacterial cells [121], or even the possibility of accessing information about the particle shape (inertial imaging) [122]. Additionally, NMS is insensitive to the charge state of the particles [123], which substantially reduces the complexity of the system as well as the data analysis. Recently, high capture area membrane resonators have been used to satisfy the compromise between achieving high mass resolution and high-throughput determination of the dry mass of intact bacterial cells (with mean dry masses around 150 fg and 470 fg, or 9.10^7 and 3.10^8 kDa, respectively) [124].

Fig. 4. (a) shows a schematic depiction of an NMS prototype system that comprises four differential vacuum stages similar to those used in Ref. [121], with a pressure gap from the atmosphere to 0.1 *Pa*. The analytes under study were in the liquid phase in a solution compatible with the electrospray ionization (ESI) technique (Fig. 4 (b)) at ambient pressure. Nebulization can also be produced by MALDI [119,120] or surface acoustic wave nebulization-SWAN [125], among other methods. The charged species are attracted to the desolvation stage, where the high temperature helps complete liquid evaporation from the nebulization stage. The transfer stage (which can contain an aerodynamic lens [125], ion guides or hexapoles [119], among others) guides the particles along the vacuum chamber at a pressure of $\sim$ 10 *Pa*. The particles flow toward the nanomechanical resonator at a pressure of $\sim$ 0.1 *Pa*. (Fig. 4 (c)). The micromechanical resonator shown in this example is a silicon nitride microcantilever. There are different transduction methods used to measure the vibration of nanomechanical resonators, ranging from electrical to optical methods [113].

Fig. 4a shows a beam deflection technique [126]. Fig. 4c shows a scanning electron microscope (SEM) image of a commercial microcantilever (Bruker, MLCT-O10) after nebulization of *Escherichia coli* bacterial cells. The microcantilever has a nominal length of 200 μm, a width of 20 μm and a thickness of 600 nm. As shown in the figure inset, acquired with tilt, the deposited bacteria show the characteristic rod-like morphology expected for *E. coli*, although vacuum conditions may introduce some degree of dehydration induced collapse. The combination of soft ionization techniques and the micromechanical resonator may be less susceptible to the fragmentation of supramolecular analytes, such as bacterial cells, viral particles or proteins, which still maintain their structural composition in a low vacuum (LV) environment.

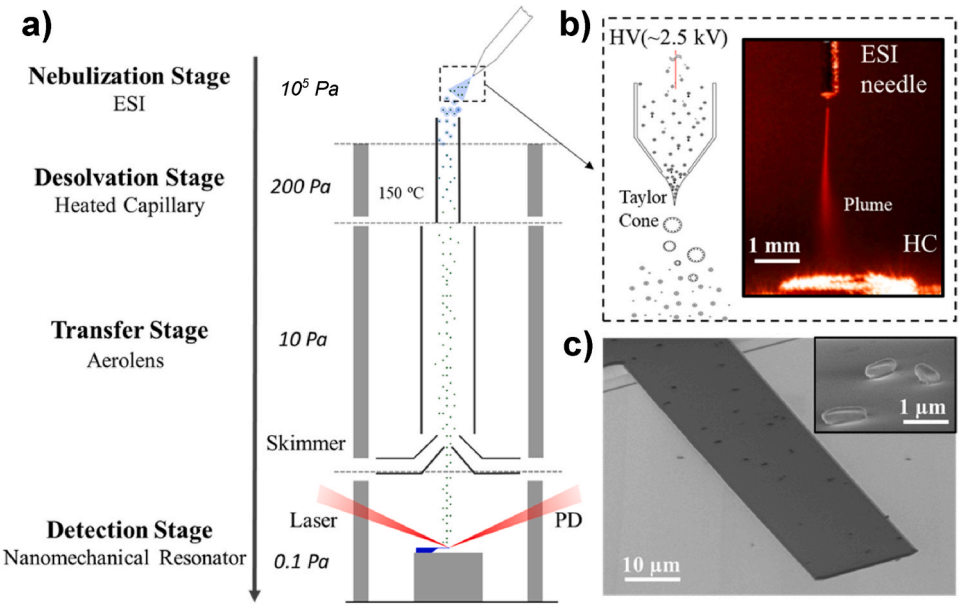

Fig. 4. Nanomechanical mass spectrometer system. a. Schematic depiction of NMS with differential vacuum stages. The analytes are nebulized at atmospheric pressure and guided to the detection stage where the sensor is placed at 0.1 Pa. The beam deflection technique is used to measure the resonator vibrations, where a laser is focused in its free-end and the reflected light is collected by a photodetector (PD). b. Electrospray ionization technique used in this prototype. c. Micro-cantilever sensor after nebulization with *E. coli*. The inset shows a zoomed image of the microcantilever surface.

Furthermore, the severe acute respiratory syndrome coronavirus 2 (SARS-CoV-2) pandemic highlights the need for new sampling techniques with high sensitivity and low time consumption. In this context, one of the greatest challenges is controlling microbiological air quality [127]. NMS has been demonstrated to measure the mass of viruses [125, 128] and the mass and stiffness of bacterial cells [121,129]. Recently, a self-focusing NMS operated in the air was used to measure the SARS-CoV-2 mass using nanomechanical resonators [130]. Furthermore, a novel optomechanical disk resonator has demonstrated its capability to measure the mass of nanoparticles and viruses [131] and the detection of vibration modes of a single bacterium [129]. The next step should be the measurement of analytes through direct air sampling, where NMS could play an important role due to its high-dynamic range and outstanding mass resolution.

4. Ion probe techniques and analytical tools

Recently, we have welcome outstanding technological advances in ion probe microscopy techniques towards nanometer resolution [132]. These ion probes operate under a HV (better than 10^{-3} Pa) and make use of charged particles with a large kinetic energy, usually hydrogen (H^+) and helium (He^+) ions. The beams are focused via magnetic quadrupoles to diameters ranging from a few tens of nanometers to a few micrometers, depending on the working characteristics of the beam line and the required beam energy and intensity. Unlike electrons, the lateral resolution of MeV ions is maintained within a few nanometers through relatively thick samples (tens of µm) [133,134], paving the way for biological materials and whole-cell (3D) structural high-resolution imaging. Furthermore, several analytical techniques can be used simultaneously.

An ion microprobe, often referred to in literature as a nuclear microprobe, is therefore used in nuclear microscopy (see Fig. 5). In customary set-ups, by scanning the beam over a region of interest of the sample, two-dimensional (2D) images of the morphological details (e.g., STIM - scanning transmission ion microscopy) and elemental distribution (PIXE – proton-induced X-ray emission) can be delivered simultaneously.

Additional depth profiling information can be extracted from the calculated beam energy loss with Rutherford backscattering spectrometry (RBS) [134,135]. Other imaging and analytical methods include

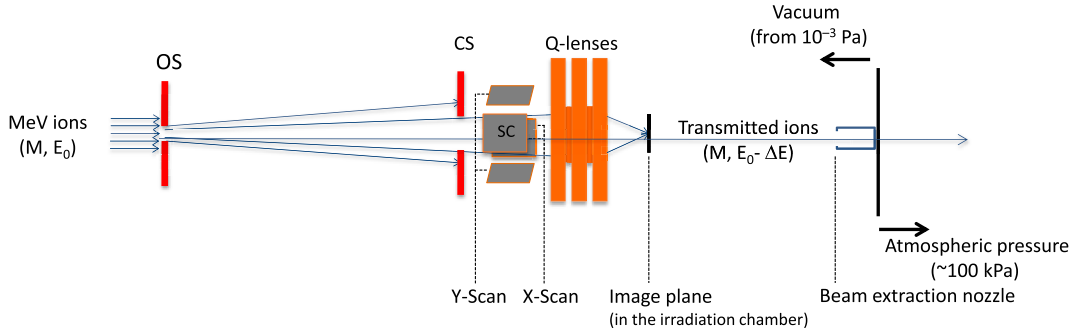

Fig. 5. Schematic of controls of a scanning transmission ion microscope from the object slit (OS) of the ion microscope to the beam extraction. The current and divergence of incident MeV ions with M mass and energy E_0 are controlled with the OS and collimator slits (CS), respectively. The sample is positioned in the irradiation chamber under vacuum at the image plane (focal plane of beam) and the beam scanned over a region of interest. The beam can be extracted to air though a thin membrane enabling microanalysis of specimens at ambient pressure. SC - scanning coils, electrostatic x,y scan module. Q-lenses - quadrupole lenses for beam focusing.

ion-induced luminescence (IL) or proton-induced fluorescence (PIF), which is not diffraction limited (the resolution achieved is only dependent on the ion beam size) [134], and MeV secondary ion mass spectrometry (MeV-SIMS) (Fig. 6) [136–138].

These techniques may be used alone or in combination with STIM or PIXE, depending on the setup. In the last decade, transnational initiatives under the scope of the European Union as part of Horizon Europe (e.g. EURO-LABS, CLEAR, ReMade@ARI/RADIATE) and the International Atomic Energy Agency (i.e., Accelerator Knowledge Portal) have opened ion probe facilities to the scientific community worldwide, which has significantly contributed to their recognition and added value in many fields of science, from biomedicine to nanotoxicology [139].

4.1. Morphological, elemental and molecular 2D analysis

One of the advantages of nuclear microscopy is that it enables the simultaneous use of different techniques to quantify the micro distributions of elements and molecules in biological materials and single cells in conditions close to pristine or in vivo (i.e., without the need for stains or contrast agents). These possibilities were applied in a variety of biomedical/environmental studies where the preservation of the original physiological conditions in vacuum assured realistic 2D microanalysis of biological samples. To ensure optimal preservation of live cells and fresh tissue structures, and to instantly halt the movement of labile elements within the typical beam range and spatial resolution of nuclear microscopy, cryo-preservation is essential. This can be achieved by using liquid nitrogen (LN) together with a cryoprotectant, such as 2-methylbutane, to quench freezing at very low temperatures, and shift water crystallization to a lower temperature range, forming vitreous ice. The cells and tissues can be stored at −80 °C until processing and further vacuum-based analysis. The subsequent procedure requires dehydration, as described below, and the method used depends on the sample type.

Several studies encompass morphological features using STIM and quantitative elemental analysis by combining PIXE and RBS (for $Z \geq 11$).

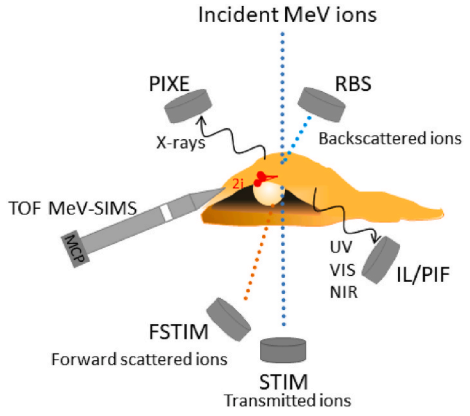

Fig. 6. Interaction of MeV ions with a biological specimen and nuclear microscopy associated techniques. **PIXE** - particle induced X-ray emission (detection of characteristic X-rays resulting from the recombination of outer shell atomic electrons with inner shell vacancies created by the impact of MeV protons). **RBS** - Rutherford backscattering spectrometry (detection of large angle backscattered ions from elastic collision of primary ions with atomic nuclei). **IL/PIF** - ion beam induced luminescence, such as proton induced fluorescence. **STIM** - scanning transmission ion microscopy (detection of the energy loss of direct transmitted ions). **FSTIM** - forward scattering TIM (detection of forward scattered transmitted ions that have been deflected off the beam axis by small angle nuclear collisions). **ToF MeV-SIMS** - Time-of-flight MeV SIMS (secondary molecular ions (2i) are desorbed from the sample surface after interaction with the MeV primary ions, accelerated toward the spectrometer and detected by the microchannel plate – MCP; time elapsed depends on the mass and charge of the molecular ion).

The state-of-the-art spatial resolution for quantitative elemental analysis at the $\mu g.g^{-1}$ dry weight level (even for tiny mass quantities corresponding to the sample volume under the micron beam resolution) is currently approximately 300 nm, whereas for STIM, it is < 30 nm. Consequently, nuclear microscopy techniques have significant advantages over SEM/TEM EDX for elemental analysis. They enable quantitative trace element mapping at part-per-million (ppm) levels in relatively thick tissue sections or whole cells, while maintaining lateral resolution. In contrast, EDX is limited by strong matrix effects and a higher bremsstrahlung background. It only provides semi-quantitative or qualitative results in the percentage range and rapidly loses depth resolution beyond a few hundred nanometers. Nevertheless, EDX remains the preferred method for routine, near-surface elemental analysis.

Therefore, quantitative elemental microdistribution helps establish relationships between compartmentalization in cells and detoxification capacity or susceptibility to pollutants in the natural environment [140,141]. Additionally, correlating endogenous biological elements with cell/tissue structures could help identify new biomarkers of disease. For example, physiological changes at the cellular level are understood in detrimental retina disorders [142,143] and Alzheimer's disease [142,143]. These findings provide insights into human pathological conditions, such as the increase in iron (Fe) concentration in specific tissue regions in skin inflammation diseases [142,143] and in atherosclerosis [144], as well as the correlation between the Zn concentration and insulin secretion in metabolic diseases [145]. In all these studies, cryoprotocols were used to guarantee that elements (electrolytes, covalently bound essential elements, or nanosized metallic complexes) and/or molecular constituents remained in their original compartments. These protocols could also ensure, to a certain extent, that the structural volume of the biological material is preserved. The usual procedure consists of quench-freezing the biological material in LN, sectioning it in a cryostat with the appropriate thickness (~10−20 μm), whenever needed, and drying it by lyophilization at ~0.1 Pa, T ~ -60 °C or dehydration in a cryostat at −25 °C under atmospheric pressure [146,147].

Although the use of chemicals or stains dramatically changes the elemental distribution in cells [148], the detection of cellular details tagged with appropriate fluorophores via IL/PIF can be used to detect fluorescence (beam currents of ~50-100 pA). Simultaneous STIM structural information with lateral resolutions of ~150 nm (using low beam currents below ~5 pA) can be useful for studying specific cellular processes associated with endo/lysosomal vesicles (200 to 400 nm in size) and their cargoes. These structures are thought to be involved in cancer metastasis and virus infection. Malaria parasites that infect human red blood cells can be detected when parasite DNA-specific fluorophores are used [134]. Major difficulties are the rapid iono-bleaching of organic dyes and the similarity between the fluorescence signal of the fluorophore and the autofluorescence of cells from endogenous fluorophores. Advances in light collection systems and in the development of stable fluorescent probes have enabled luminescence imaging and simultaneous mapping of cellular structures with a spatial resolution of sub 30 nm in whole-cell volume [134]. Recent developments in correlative ion-beam-induced and structural microscopy have brought nuclear microscopy close to the spatial resolution of STED/4Pi super-resolution microscopy (<50 nm). While IL/PIF lacks molecular specificity and is not suitable for live-cell imaging, both approaches rely on bright, photostable probes. Optimized probes will enhance imaging efficiency and expand the complementary use of these microscopy modalities in biological samples.

During the last decade, significant advances in the exploitation of focused high-energy, heavy ions (e.g., oxygen and chlorine) have opened the possibility of obtaining higher yields of non-fragmented, large molecular secondary ions (>10 kDa) suitable for the molecular imaging of biological materials with much higher spatial resolution than is currently possible with laser techniques such as MALDI [136]. The submicrometer focusing of the low-current primary ion beam allows

simultaneous molecular and structural (STIM) mapping of the biological tissue on a subcellular scale (500–800 nm) when operating in a vacuum [136,149]. The 2D chemical imaging capabilities of the MeV-SIMS method have been demonstrated in freeze-dried cultured cells and plant materials. Biologically relevant ionic species, e.g., Na^+ and K^+, and lipid fragments have been mapped in CaCo-2 cells [150], whereas in cannabis leaves, medically valuable cannabinoids can be imaged and discriminated (e.g., anti-inflammatory/neuroprotective effect molecules versus psychoactive molecules) [150]. MeV-SIMS can also be performed simultaneously with heavy ion PIXE measurements, which may help eliminate some of the ambiguity of matrix interferences in the mass spectra. Recent developments have enabled the detection and imaging of organic molecules under atmospheric pressure, without the high-vacuum chamber ($\sim 10^{-5}$ Pa) required in conventional MeV-SIMS systems [150,151]. In this setup, the primary ion beam is extracted into air to sputter secondary ions from the sample, which are then carried by a helium gas flow into the mass spectrometer [152]. However, the ability to identify organometallic molecules in biological materials via MeV-SIMS along with the quantitation of metallic atoms via PIXE remains to be verified.

4.2. Advances in nanotoxicology using nuclear microscopy toward 3D resolution measurements

One of the most interesting current possibilities of 3D approaches in nuclear microscopy resides in the field of nanotoxicology. Nuclear microscopy offers unique analytical potential for examining the subsurface layers of relatively thick samples, retrieving the depth-dependent profile of the elements detected and reconstructing three-dimensional (3D) images of that sample. 3D reconstruction can be achieved by exploring RBS data [151,152] or by performing tomography via STIM and PIXE [153]. This approach is particularly attractive for detecting the distribution of metallic nanosized particles or molecules in tissues and whole cells and studying biointerfaces.

Early studies demonstrated the safety of the use of nanosized TiO_2 and ZnO particles as physical agents in sunscreens by establishing permeation profiles in the skin [154,155]. However, more recent approaches involving cellular and organism models have shown how different geometries and metal contents of nanosized TiO_2 nanoparticles influence their internalization in epithelial and endothelial cells, with an impact on the essential element contents and metabolism of cells [156]. Additionally, nanosized Ti in ecosystems could be toxic to zooplankton, which plays an important role in aquatic food chains, and influences the expression of specific proteins involved in reproduction [157]. Additionally, monitoring the dynamics of the biodispersion of SiC nanoaerosols in rat lungs could aid in understanding clearance dynamics, which is highly important for assessing the safety of nanosized materials in the context of occupational and environmental health [158].

The visualization of individual gold (Au) nanoparticles of 100 nm in diameter in whole cells via STIM at low ion currents and at a probe lateral resolution of 25–30 nm represented a breakthrough for high-resolution nuclear microscopy [151]. The analysis of the ion beam energy loss through the RBS spectra enabled the resolution of the Au nanoparticles at the cell surface and those inside the cell. These results paved the way to improve depth profiling capabilities, translating backscattered data into a true 3D display of the elemental distributions in the whole-cell volume, even for routine analysis conditions with relatively high ion currents (~100 pA) and lateral submicrometer resolution. The 3D model of the concentration of one element of interest can be constructed by correcting the number of events for each depth layer defined for the RBS spectra with the stopping power (beam energy loss in the ion path across the cell) and the variation in the scattering cross section through the cell [152].

This approach is particularly useful in toxicity studies of nanosized entities (metallic particles and complexes) in vitro, as both their amount and location can be resolved in freeze-dried whole cells plated onto a 100 nm thick silicon nitride window. By using 2.0 MeV helium ion beam, a fully 3D cell volume reconstruction with 50 nm depth resolution was obtained, confirming the assimilation of CuO nanoparticles (with a mean diameter of ~20 nm) into *Saccharomyces cerevisiae* (Fig. 7) [152]. In most biological matrices, only elements with $Z > 20$ can be securely used to reconstruct 3D models with RBS spectra. The mass of the projectile influences the depth resolution achieved, as it depends on the energy loss of the ion in its path through the sample. Protons (^1H ions) can probe further in a sample at a cost of lower depth resolution than can heavier ions, such as ^4He ions. The latter enables an increase in depth resolution and consequently in the number of depth layers describing the biological sample. The concentration of the element of interest may also influence the quality of the depth profile model, as it depends on spectral statistics.

This methodology is attractive for identifying the localization of metallic nanosized complexes in cells, which are not easily differentiated by density. This is the case for metallic nanoparticles, which are usually analyzed via TEM, SEM or STIM approaches. For example, the cellular localization of new potential anticancer drugs constructed with bioactive ligands and a coordinated transition metal is being studied.

The rationale behind this is the development of drugs with high specificity and toxicity for tumor cells while preserving healthy counterparts. Therefore, by studying the distribution of the metal (present in the organometallic complex) in the whole-cell volume (i.e., PIXE mapping and RBS depth profile), the complex uptake and preferential targets (e.g., membrane, cytoplasm, and nucleus) can be characterized, as illustrated in Fig. 8 [159,160].

Tomographic reconstruction on the basis of ion energy loss (STIM) and the number of detected X-rays for each chemical element (PIXE) could be an alternative to evaluate the interaction of nanosized dense particles with unicellular organisms as good quality density images [161,162], and satisfactory quantitative results for metals can be achieved [153,162,163]. Recent advances in STIM and PIXE tomography have provided adequate quantitative results for essential elements and discrete metal inclusions corresponding to metallic nanoparticles internalized by the *Caenorhabditis elegans* nematode [153]. Therefore, the application of STIM and PIXE tomography in nanotoxicology studies involving more realistic models, such as 3D bioengineered tissues or organs, has become highly appealing.

5. Toward nearly atmospheric/environmental electron techniques

The principle of operation of electron techniques working with samples standing in mild vacuum is the creation of sharp pressure gradients through tiny diameter-controlled nozzles/pinholes (fourth column, Table 2). The vacuum chambers are divided into several regions separating the one with low pressure where the sample stands and the HV/UHV ones where the electrons travel. Differential pumping systems are responsible for ensuring the necessary pressure gradients, and the reduced volume between the sample and the excitation/scape pinhole prevents the total decay/absorption of electron populations. These differences apply to electron microscopy systems, where high-energy electrons impinge the sample for excitation, and photoelectron spectroscopy systems, where X-ray-induced photoelectrons are collected and analyzed. A view of the instrumentation is shown in Fig. 9 for the environmental scanning electron microscope (ESEM) and wet scanning transmission electron microscope (wetSTEM), and in Fig. 10 for the near ambient pressure X-ray photoelectron spectrometer (NAP-XPS). The typical working pressure at the sample region of these systems is 100–1000 Pa, which can be reached, for the characterization of biological samples, with a water partial pressure. Imaging in these microscopes is granted by secondary ionization cascade electrons produced when low-energy secondary electrons impact water vapor molecules (Fig. 9). An additional general advantage is that the atmospheric conditions at the sample side act as a discharging environment so that

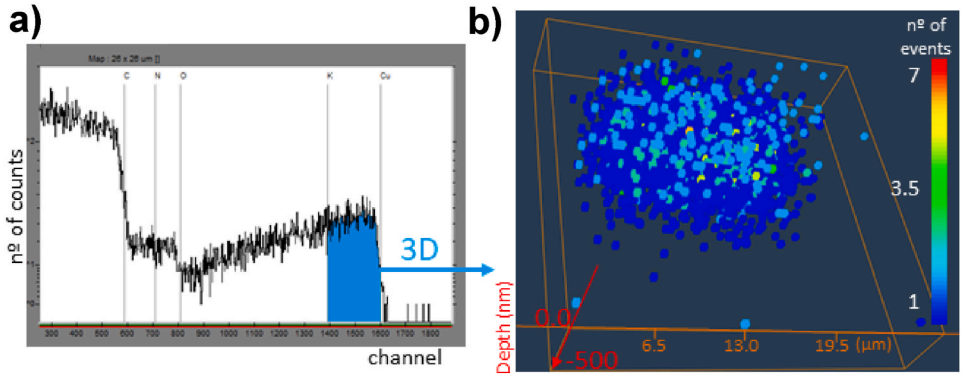

Fig. 7. a) - RBS spectra obtained in a 26 × 26µm^2 scan of a *Saccharomyces cerevisiae* cell using 2.0 MeV helium ions. The section used in the 3D analysis is in blue, and is defined by the surface barrier of the chosen limit elements, i.e., potassium as the relevant matrix element with highest Z, and Cu. b) - The 3D model of the yeast cell with 50 nm depth resolution highlights a significant Cu uptake by the cell. The amount of Cu (nanoparticles) is expressed as n° of events (corrected for beam energy loss at different depths) and represented by a color gradient: low–blue to high–red. The cells were incubated with CuO nanoparticles in a concentration of 40 mg Cu/L of culture medium. The 3D model was created using MORIA software. Model parameters: cell density 1.2 g/cm^3; energy depth calibration = 0.404 keV/nm; maximum depth probed = 496 nm; 11 layers. Data was compressed to 128x128 pixels/layer. (For interpretation of the references to color in this figure legend, the reader is referred to the Web version of this article.)

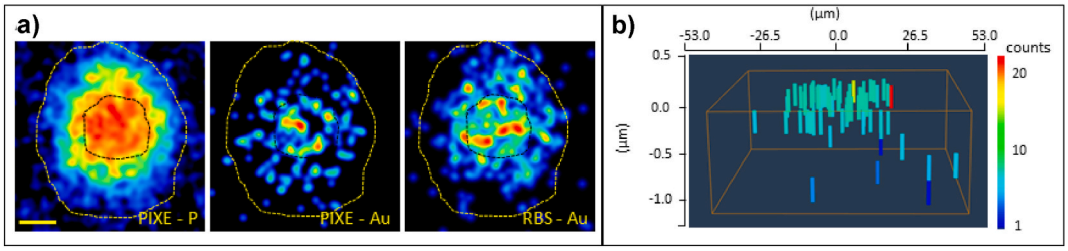

Fig. 8. a) Nuclear microscopy images of P and Au distribution obtained from the PIXE and RBS spectra of a cell (human prostate cancer cell line, PC3) incubated with Auranofin, a Au complex already used as a medication. The dotted line indicates the cell contour and the central nucleus rich in P. Au is evenly distributed in the cell. The amount is represented by a color gradient with a dynamic scale: low–blue to high–red. Scale bar, 5 µm. b) 3D representation plot of the model distribution of Au in the cell depicted in a), obtained with a 2.0 MeV proton beam. A four-layer model with a depth resolution of 300 nm/layer shows that Au was internalized by the PC3 cell. The amount of Au does not differ significantly through cell depth, suggesting that Au is mainly located in the cell cytoplasm and cell core. Data in layers were compressed to 64 x 64 pixels to better visualize the Au distribution inside the cell. The box represented in the plot sets the point of view and the perspective of the cell in (A) where zero indicates the surface of the cell. The relative amount of Au in the cell in number of counts is represented by a color gradient. (For interpretation of the references to color in this figure legend, the reader is referred to the Web version of this article.)

typical image saturation (for electron microscopes) or spectral shifts (for photoelectron spectrometers) due to charging are avoided in these configurations. The consequence is that sample preparation is much more straightforward. Despite these advantages, caution should be taken when considering artifacts since the observed/analyzed matter is exposed to radiation, and biomolecules may overpass their radiation damage threshold. The presence of water increases the probability of indirect radiation damage due to interactions with water-derived radicals.

In ESEM and wetSTEM (Fig. 9), the critical chamber from the point of view of vacuum is at the generation of the electrons (electron gun chamber). On their way to the sample chamber, the electrons pass through several pressure-limiting apertures, saving a pressure gap from $\sim 10^{-5}$ to $\sim 10^{3}$ Pa. Further details on the instrumentation can be found in the specialized bibliography, which also emphasizes detector technology depending on the operation mode, gas/water vapor control and holder temperature regulation [164]. On the other hand, for the NAP-XPS system (Fig. 10), the critical point is the extraction of the X-ray ejected photoelectrons, which travel from the sample chamber to the electron energy analyzer through an inverse and even more acute pressure gap from $\sim 10^{3}$ to $\sim 10^{-7}$ Pa. For this technique, the process is efficient as long as the path of the probed electrons in the sample chamber is minimal (<0.5 mm), which justifies the proximity of the nozzle/pinhole to the sample.

Further comments on critical developments, such as the incorporation of specialized electron transfer optics, differential vacuum stages and gas pressure control at the sample chamber, can be found in previous reviews (note that the technique is also referred to as atmospheric pressure photoelectron spectroscopy, APPES or APXPS) [21, 165].

5.1. Applications of ESEM/wetSEM to biointerfaces

Electron microscopes operating under wet conditions are essentially applied to the moisture conditions of environmental scanning electron microscopes (ESEMs). These studies opened the use of electron microscopes at 10–100 Pa and cooling at 2–8 °C, which lead to approximately 50% relative humidity, that is, to environments closer to natural conditions in terms of potential to preserve structural water. The application of different modes of SEM operation to plants has been reviewed, highlighting operation modes to optimize the acquisition of images from structures of different nature (cellulosic, wax, and cell) [166]. In fact, in these systems sample preparation may be as simple as directly exposing on an appropriate support. Examples of imaging possibilities with the ESEM are shown in Fig. 11.

The imaging capabilities have even increased with nanomechanical measurements combined with microcantilever probes, which have been used to characterize yeast elastic properties [167]. The most relevant aspect is, however, the possibility of studying functional dynamic processes, such as swelling of hydrogel adhesive pads in algae [168] or

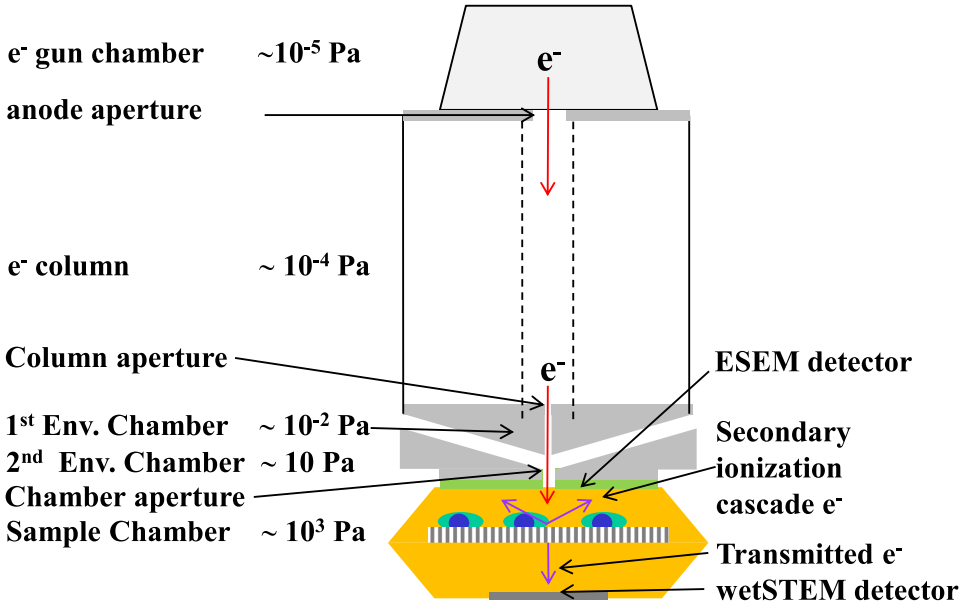

Fig. 9. Schematic representation of an environmental scanning electron microscope allowing the observation of samples at pressures on the order of 10^3 Pa, while primary electrons are produced at 10^{-5} Pa. The column and chamber apertures are responsible for sustaining the differential pressure, allowing the transport of high-energy electrons (keV). Secondary electrons create an ionization cascade and derived electrons can be collected and analyzed to produce SEM images. For thin samples, a scanning transmission electron microscopy configuration is also possible under quasi-environmental conditions.

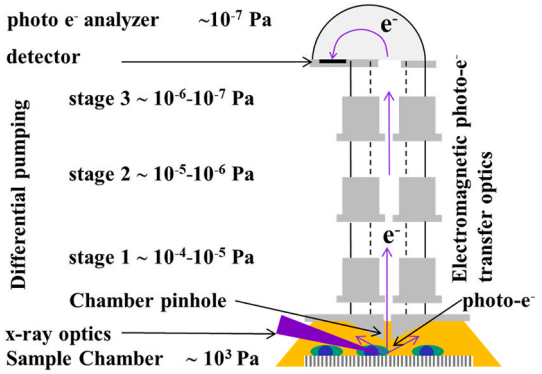

Fig. 10. Schematic representation of a nearly atmospheric pressure X-ray photoelectron spectrometer (NAP-XPS) allowing the analysis of surfaces at pressures of the order of 10^2 Pa, while photoelectrons are analyzed at 10^{-7} Pa. The chamber pinhole and the differential pressure along the photoelectron transfer optics are responsible for sustaining the pressure gap, allowing the transit of low–mid-energy electrons (0–1000 eV).

opening of stomatal pores in leaf tissue [169]. These studies extend further to the characterization of mammalian cells, revealing, for example, microtopographic features of organelles in osteoblast cells with no fixation, drying or metallic coating and no sacrifice of the mechanical integrity of the cells [170].

The parallel use of energy dispersive X-ray spectroscopy can be exploited to determine the effects of different biocement formulations on the induction of bone growth in the medullar cavity for different Ca/Si ratios of the cement [171]. However, the cells are not alive after measurement, which limits the potential applications of ESEM with respect to other optical methods, especially for dynamic studies, such as for the determination of cell viability in different chemical/biochemical/pharmacological environments [172].

The scanning transmission configuration of the electron microscope has also evolved to work at high pressures and is mostly known as wetSTEM, owing to its most generalized working conditions using water. The first bioanalytical studies using wetSTEM were devoted to observing carbon storage in bacteria [173]. Other prokaryotes (tobacco mosaic virus) have been studied in alternative wetting liquids [174]. This study leaves the path open for the study of the SARS-CoV-2 virus under analogous conditions, which has already been observed at low magnification via standard SEM [175]. The layering of vesicular structures has been studied in synovial fluids by following an electron microscopy multitechnique approach, including wetSTEM [22]. Further developments have allowed correlation experiments with fluorescence microscopy to localize the receptors of a marker related to the aggressiveness of breast cancer. This requires special labeling with QD-antimarker conjugates, ensuring fluorescence activity after electron irradiation and good atomic mass contrast [176]. It has been recently shown that wetSTEM allows the characterization of hydrophilic/hydrophobic samples at very different ranges of water content/interaction. This possibility has been exploited to analyze in a pore by pore approach the water adsorption and desorption processes of organosilane biofunctionalized columnar porous silicon [177], which suggest that this system could be used to validate reusability/aging of bioanalytical systems. Possible uses for these porous systems may consider the possibility to transfer through controlled permeability tiny amounts of hydrated molecules (i.e. wet proteins) to an ion/electron analysis surface, which could be a complementary approach to membrane capsules described in section 5.3 in which transfer of ions/electrons through the membrane is possible, meanwhile the membrane remains impermeable to molecules.

5.2. *NAP-XPS applications to biointerface analysis*

The advances in photoelectron spectroscopy under nearly atmospheric conditions are more recent than those in electron microscopy because of the UHV operation conditions of a photoelectron analyzer. The pressure difference with respect to the typical analysis conditions is greater, as is the increasing technological challenge of the required differential pumping system. The technological gap has been filled with new equipment during the last decade, and new applications of NAP-XPS are increasing. Several applications are illustrated in Fig. 12. As a proof of interest for the field of biointerfaces, this technique has been used to characterize diverse solid–water interfaces, revealing the O 1 s

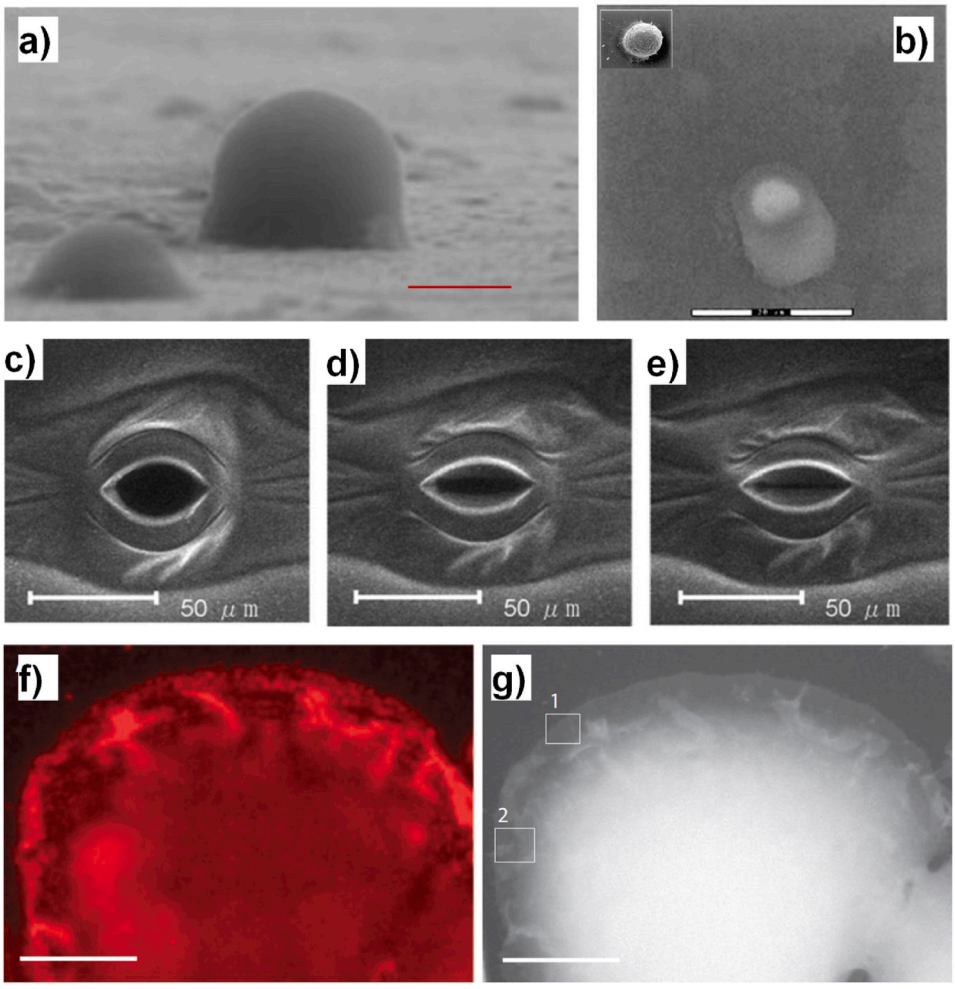

Fig. 11. ESEM imaging of biological units from different species. a) Yeast cell imaged at 11 °C, 400 Pa and 60% relative humidity in a system allowing mechanical testing. The scale bar is 2 μm. b) ESEM image of an *Enteromorpha* spore in its natural hydrated state at vapor pressure 600 Pa and 2 °C. Note natural enveloping layer. Inset shows the image in standard SEM conditions with striated adhesive layer and overall volume reduction. Common scale bar is 20 μm. c-e) Sequence of ESEM images showing the closure of a stomatal pore (relative humidity from 97% to 91% at 7-8 °C). f-g) Correlative fluorescence (f) and ESEM (g) images of a breast cancer cell with edge ruffles (scale bar represents 10 μm).

spectrum of water vapor [178]. The advantages of operating at 10^3–20.10^3 Pa water vapor pressure are threefold: a) the sample stands in a conducting environment so that charge shifts in binding energy are strongly minimized (if present), b) the sample is much closer to its natural hydrated state, which helps preserve its biomolecular structure, and c) the preserved water shells in the biomolecules help protect its structure from direct radiation damage [179]. This latter effect is favored by the efficient radiation energy dissipation that may however increase locally the presence of derived free radicals as secondary effect. Bearing all these aspects in mind, one would expect to see studies on dynamical–operando processes, analogous to those performed on inorganic catalytic systems, but with enzymatic reactions. Currently, the use of NAP-XPS has reached the barriers of biointerfaces in relatively simple problems, such as the characterization of bacterial membranes [180], biopolymers such as cellulose and hydrogel biomaterials [179], naturally biomineralized tissues [181] or the study of the biofunctionalization cascade of a dual biosensor incorporating gold nanoparticles [182]. Recently, a systematic study has analyzed the effects of the water partial pressure on the analysis of adsorbed fibrinogen on hydrophilic and hydrophobic surfaces. The analysis protocols establish how to minimize derived sample damage. Furthermore, different x-ray excitation energies give rise to photoelectrons with different kinetic energies that can emerge from deeper areas of the sample. Thus, by comparing the core level spectrum of one element at different excitation energies, an in-depth analysis can be carried out with depth inspection ranges from a few nm (soft x-rays) to several tens of nm (hard x-rays). By following the intensity of hydrophilic and hydrophobic related queues in the C 1 s core level spectrum of the proteins, it could be confirmed that, on hydrophilic supports, the fibrinogen exposes hydrophobic queues to the outer surface, which agrees with the expected conformation to minimize surface free energy at the support-protein biointerface [183].

5.3. *Analysis of biointerfaces by encapsulation*

An alternative to differential pumping instrumentation exists in the form of enclosing sample capsules with specific electron-transparent membranes. The general scheme of the working principle of these membrane capsules is presented in Fig. 13. Wet analytes can be hermetically closed in microporous cavities, which are subsequently sealed with an ultrathin Si_3N_4 slab or a few layers of graphene (or other 2D materials) [184,185]. The thickness of the Si_3N_4 ranges from a few tens of nanometers until hundreds of microns depending on the energy and nature of the probing particle. Si_3N_4 withstands better than graphene the sputtering induced by ions but graphene is thinner and more transparent to electrons, increasing the signal for electron-based systems. Examples of imaging in different modes (backscattering, low energy) are available in Fig. 14a–b.

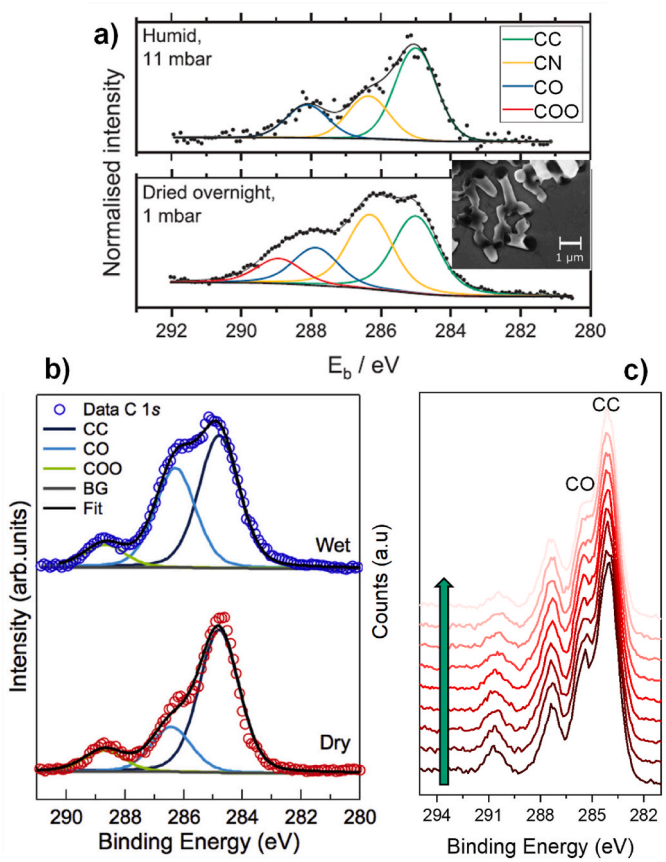

Fig. 12. a) C 1s XPS spectra from *Escherichia Coli* acquired in different conditions. Significant relative intensity changes with respect to aliphatic CC peak are observed for carbonyl (CO), amide (CNO) and carboxyl groups (COO). Note inset image denoting induced damage. b) C 1 s core-level region and corresponding peak components of wet (blue) and dehydrated (red) hydrogel contact lens measured in ambient air at 100 Pa (BG-background). c) Cumulative C 1 s core level spectra acquired in NAP-XPS mode at 200 Pa H_2O partial pressure from fibrinogen adsorbed on a perfluorosilane. The spectra evidence progressive direct and indirect beam damage (follow arrow and peak widening with loss of CC-CO resolution. Note CC reference centered at 284 eV in this latter case). (For interpretation of the references to color in this figure legend, the reader is referred to the Web version of this article.)

This promising approach has proven to be efficient in the operando characterization of catalytic systems. Additionally, tissues have been observed by SEM in fully wet conditions, although contrast in the tissue had to be enhanced by heavy element staining and observation in backscattered electron mode [19]. The images distinguished the nuclei and organelles in the cells of the kidney sections from their membranes and surrounding red blood cells. A comparison of the advantages of different microscopic techniques and different staining methods has also been conducted on the basis of observations of *Trypanosoma Brucei* [186]. This type of cell is also compatible with STEM, which allows the use of gold nanoparticles as contrast elements to target *Escherichia coli* membranes or fibroblasts (COS7) at the receptor level [20]. Other examples include observation with enhanced contrast by using gold-labeled selective cell sites. In fact, epidermal growth factor receptor

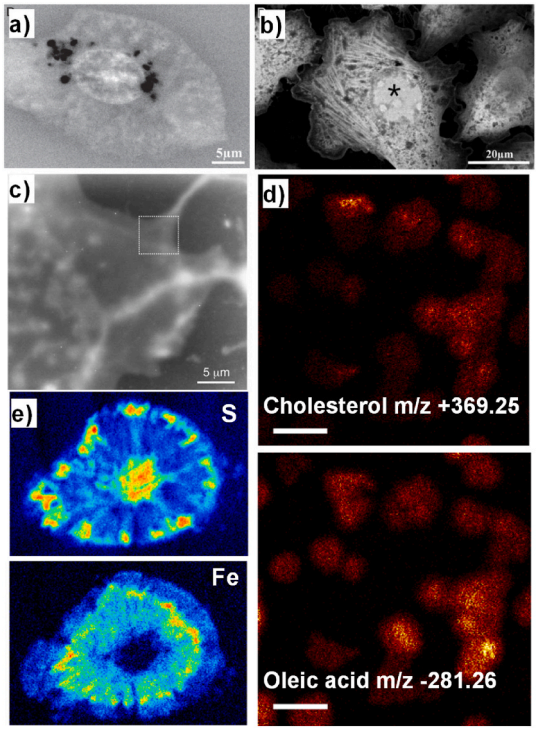

Fig. 14. a) SEM imaging through encapsulating membranes in backscattering detection mode. Untreated Chinese hamster ovary (CHO) cell grown on a fibronectin-coated polyimide partition membrane in normal growth medium and no staining. b) Low energy SEM image showing Actin fibers from CHO cells stained in uranyl acetate. Asterisk denotes the nucleus. c) Wet cell STEM imaging of gold-labeled epidermal growth factor receptors in monkey kidney fibroblast-like cells within a Si_3N_4 capsule. d) ToF-SIMS images of graphene-covered untreated human lung carcinoma cells cultured on a wet support. Scale bars represent 100 µm. e) Qualitative elemental maps of *Porcellio scaber* internal gland cross section with visible cells and internal structure. Sample in frozen-hydrated state between two polymer foils. Scan area 500 × 500 μm^2. Top: S and bottom: Fe signals. (For interpretation of the references to color in this figure legend, the reader is referred to the Web version of this article.)

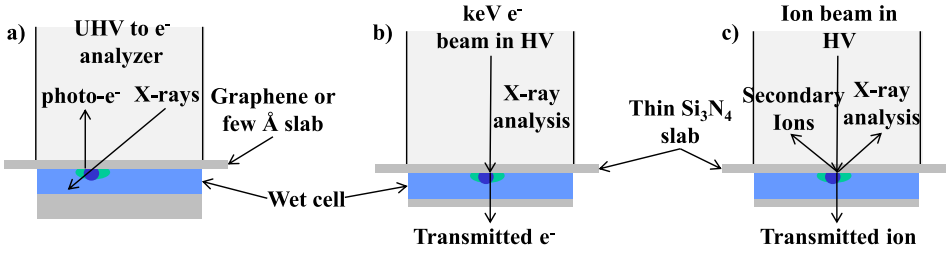

Fig. 13. Scheme of the working principle for the biointerface analyses working with encapsulating membranes. Electron/ion transparent membranes are required on a single side for XPS analyses since the excitation X-rays and probed electrons travel through the UHV chamber (a). Identical scheme corresponds to SEM systems. For TEM and STEM, transmitted electrons require two electron transparent membranes to isolate the wet sample from the vacuum chamber at the incident and transmitted electron chamber (b). Similarly, two ion-transparent membranes are required for STIM (c) Secondary ions and emitted X-rays allow supplementary analysis in backscattering configuration.

could be immune-recognized in monkey kidney fibroblast-like cells, which were then encapsulated within 50 nm thick Si_3N_4 windows (Fig. 14c) [20]. Some progress made by observation in TEM could further bring progress to observation in SEM, STEM and STIM microscopies. Examples of visualized biological objects using encapsulation are shown in Fig. 14d-e. For instance, the wet compartment has evolved to the limit of allowing observation through a flowing liquid, which has been applied to the holographic reconstruction of magnetotactic bacteria [187]. More relevantly, organelles and the dynamic evolution of vesicles have been observed in prostate cancer cells with no embedding, dehydration or staining [188]. A critical point in this liquid cell for TEM operation is working at extremely low electron doses of approximately 2–5 electrons per nm^2 to avoid electron beam damage to the biomolecular structures. At nanomolecular level, it has allowed to characterize DNA−Au nanoparticle conjugates, whose 3D motion could be monitored in a graphene liquid cell [189].

The encapsulation approach has been also used for analysis with ion probes of different energies. For example, Hua et al. [190] used an ion beam to drill a microcavity in a microfluidic system based on a silicon nitride membrane with a system disposed very much like as depicted in Fig. 13c (but with limited volume in the cell chamber controlled by microfluidics) so that they could interrogate directly the cell, detecting Zn ions from the cytosol, which was related to previous internalization of ZnO nanoparticles. Recently, the innovative protocol based on the use of a single-layer graphene to prepare biological samples has been applied to ion systems [18] as previously done for TEM and SEM experiments [191]. It allowed to successfully observe the distribution of cell membrane lipids (i.e., cholesterol) and fatty acids (i.e., palmitic acid) through a microhole in the graphene layer. The authors also demonstrated that cell viability is maintained both after the capping of the graphene layer and under vacuum, allowing both affinity purification-MS and ToF-SIMS imaging with submicron lateral resolutions [18]. As underlined by H. Heeren, this approach opens a wide range of possibilities for the use of MSI techniques to further investigate the chemical dynamics and wet catalytic reactions of the cell membrane [192].

For ion probe techniques, the approach is typically based on the use of an external beam extracted directly from a high-vacuum system through a silicon nitride window, as illustrated in Fig. 13 (c). ToF-SIMS has, for example, been used to characterize water clusters while running water through a microfluidic device [193]. From this technical success applications to biological systems include differentiation of lipid distributions in human carcinoma cells (Fig. 14d). Other procedures, stemming from electron microscopy, enable microanalysis of tissues in a frozen-hydrated state in conditions near to atmospheric pressure inside the measuring chamber under vacuum by tightly encapsulating the tissue with two precooled polymer foils [194,195]. A relevant example is illustrated in Fig. 14e. This method is particularly attractive for studying elemental distributions in vacuole compartments of plant cells, which become void after water removal by freeze-drying or cryo-dehydration, and in labile organisms, such as planktonic species [146,195].

6. Conclusions and perspectives

The use of electron and ion techniques for the analysis of biological structures and the exploration of the interfaces between different molecular structures can be considered a classical topic. However, the current state of the art underlines the need for converging to analyses in conditions closer to the native environment of the biological samples. From samples analyzed in HV or UHV, technology has moved on to different alternatives to avoid sample denaturing, which takes place mainly by loss of structural water. Although the analysis in pure natural conditions is only attainable in particular cases with ion probing, current developments in the control of vacuum systems converge to the analysis of biological matter in its natural state.

A first alternative concerns cryogenic sample preparation and observation. Both steps are critical to ensure that no drastic phase separation takes place during sample preparation and that little radiation damage occurs during analysis (as far as it can be identified). With the required precautions during operation, we have shown that remarkable results can be extracted from cryo microscopies and spectroscopies based on both electrons and ions.

Secondly, we have shown that differential vacuum control is key for several biointerfaces challenges. In combination with nebulization and ionization systems, we have shown how nanomechanical mass spectroscopy allows us to identify full single organisms in an unprecedented manner, providing additional data regarding the single cells detected, such as density and mechanical properties.

We have also shown that recent instrumentation allows creating vacuum gradients through differential pumping and nozzle interconnected chambers in microscopes and spectrometers to make compatible the short travelling distance of ionized matter at mild vacuum with the analysis of biomolecular samples at water partial pressures of 10000-1000 Pa. Under these conditions, retention of the less strongly bound water molecules cannot be ensured and special protocols to minimize radiation damage (especially indirect effects) should be applied since free radicals out of cryogenic conditions present a high mobility within the specimen. As a third strategy, we have shown that appropriate electron/ion transparent materials can be used to encapsulate the biointerfaces of interest (even in microfluidic flow conditions) and provide imaging and spectroscopic relevant information. Precautions in this approach regard the stability of the membrane, whose degradation could derive in system damage by sudden increase of pressure. The above-mentioned cautions regarding sample degradation due to exposure to radiation also apply.

By the incorporation of this instrumentation advances, scientists have induced unprecedented outbreaks such as reliable chemical imaging of cells and tissues with potential for identification of foreign bodies, new records in the mass limit detection of single units in mass spectrometers, structural 3D mapping and biodistribution of drugs, water porosimetry in biofunctionalized materials and protein conformation details upon adsorption to hydrophilic vs hydrophobic surfaces. The potential for transformation of spectral information into images and, reciprocally, the transformation of images into quantitative data, reinforce the idea of the relevance of the described instrumentation for biointerface characterization.

CRediT authorship contribution statement

Oscar Malvar: Writing – review & editing, Writing – original draft, Conceptualization. **Giacomo Ceccone:** Writing – review & editing, Writing – original draft, Conceptualization. **Paulina Rakowska:** Writing – review & editing, Writing – original draft, Conceptualization. **Miran Mozetič:** Writing – review & editing, Writing – original draft, Conceptualization. **Teresa Pinheiro:** Writing – review & editing, Writing – original draft, Conceptualization. **Miguel Manso Silván:** Writing – review & editing, Writing – original draft, Conceptualization.

Declaration of competing interest

The authors declare that they have no known competing financial interests or personal relationships that could have appeared to influence the work reported in this paper.

Acknowledgments

Oscar Malvar acknowledges the service from MiNa Laboratory at IMN, and founding from EU (FEDER, FSE), MCIN/AEI/10.13039/50110001.1033 and Next Generation EU/PRTR (EQC2021-006944-P). T. Pinheiro acknowledges funding from UIDP/04565/2020 (iBB/IST) and LA/P/0140/2020 (i4HB) and from International Atomic Energy Agency (IAEA) Coordinated Research Project “Sub-cellular imaging and

irradiation using accelerator-based techniques" CRP F11024, Research contract n° 26800. M. Manso-Silván thanks project PID2023-151371OB-C22 funded by MCIN/AEI/10.13039/501100011033 and FEDER, EU, grant FLASHOnChip (PLEC2022-009256) by MCIN and ASAP-CM (P2022/BMD-7434) from DGI-Comunidad de Madrid. M. Mozetič acknowledges support from the Slovenian Research Agency, grant #P2-0082. Paulina D Rakowska acknowledges funding form the 3D OrbiSIMS project in the Life Science and Health Programme of the National Measurement System of the UK Department of Business, Energy and Industrial Strategy and from the 15HLTH01 MetVBadBugs project of the EMPIR Programme co-financed by the Participating States and from the European Union's Horizon 2020 Research and Innovation Programme.

References

[1] A. Zsom, S. Seager, J. de Wit, V. Stamenkovic, Toward the minimum inner edge distance of the habitable zone, Astrophys. J. 778 (2013) 109.
[2] E. Keles, J.L. Grenfell, M. Godolt, B. Stracke, H. Rauer, The effect of varying atmospheric pressure upon habitability and biosignatures of Earth-like planets, Astrobiology 18 (2018) 116–132.
[3] M. Mozetic, A. Vesel, G. Primc, C. Eisenmenger-Sittner, J. Bauer, A. Eder, G.H. S. Schmid, D.N. Ruzic, Z. Ahmed, D. Barker, K.O. Douglass, S. Eckel, J. A. Fedchak, J. Hendricks, N. Klimov, J. Ricker, J. Scherschligt, J. Stone, G. Strouse, I. Capan, M. Buljan, S. Milosevic, C. Teichert, S.R. Cohen, A.G. Silva, M. Lehocky, P. Humpolicek, C. Rodriguez, J. Hernandez-Montelongo, D. Mercier, M. Manso-Silvan, G. Ceccone, A. Galtayries, K. Stana-Kleinschek, I. Petrov, J. E. Greene, J. Avila, C.Y. Chen, B. Caja-Munoz, H. Yi, A. Boury, S. Lorcy, M. C. Asensio, J. Bredin, T. Gans, D. O'Connell, J. Brendin, F. Reniers, A. Vincze, M. Anderle, L. Montelius, Recent developments in surface science and engineering, thin films, nanoscience, biomaterials, plasma science, and vacuum technology, Thin Solid Films 660 (2018) 120–160.
[4] P. von Paris, P. Hedelt, F. Selsis, F. Schreier, T. Trautmann, Characterization of potentially habitable planets: retrieval of atmospheric and planetary properties from emission spectra, Astron. Astrophys. 551 (2013) A120.
[5] R.F. Thompson, M. Walker, C.A. Siebert, S.P. Muench, N.A. Ranson, An introduction to sample preparation and imaging by cryo-electron microscopy for structural biology, Methods 100 (2016) 3–15.
[6] R.E.A. Williams, D.W. McComb, S. Subramaniam, Cryo-electron microscopy instrumentation and techniques for life sciences and materials science, MRS Bull. 44 (2019) 929–934.
[7] J. Watt, D.L. Huber, P.L. Stewart, Soft matter and nanomaterials characterization by cryogenic transmission electron microscopy, MRS Bull. 44 (2019) 942–948.
[8] M.J. Zachman, N. de Jonge, R. Fischer, K.L. Jungjohann, D.E. Perea, Cryogenic specimens for nanoscale characterization of solid-liquid interfaces, MRS Bull. 44 (2019) 949–955.
[9] K. Abe, Y. Fujiyoshi, Cryo-electron microscopy for structure analyses of membrane proteins in the lipid bilayer, Curr. Opin. Struct. Biol. 39 (2016) 71–78.
[10] N. Xia, J.S. Shumaker-Parry, M.H. Zareie, C.T. Campbell, D.G. Castner, A streptavidin linker layer that functions after drying, Langmuir 20 (2004) 3710–3716.
[11] D.G. Castner, B.D. Ratner, Biomedical surface science: foundations to frontiers, Surf. Sci. 500 (2002) 28–60.
[12] B. Kasemo, Biological surface science, Surf. Sci. 500 (2002) 656–677.
[13] A. Shchukarev, M. Ramstedt, Cryo-XPS: probing intact interfaces in nature and life, Surf. Interface Anal. 49 (2017) 349–356.
[14] D. Baer, M. Camci, D. Cant, S. Chambers, H. Cohen, P. Gokturk, D. Morgan, A. Shchukarev, P. Sherwood, S. Suzer, S. Tougaard, J. Watts, What more can be done with XPS? Highly informative but underused approaches to XPS data collection and analysis, J. Vac. Sci. Technol. A 43 (2025) 040801.
[15] J.T. Zhang, J. Brown, D.J. Scurr, A. Bullen, K. MacLellan-Gibson, P. Williams, M. R. Alexander, K.R. Hardie, I.S. Gilmore, P.D. Rakowska, Cryo-OrbiSIMS for 3D molecular imaging of a bacterial biofilm in its native state, Anal. Chem. 92 (2020) 9008–9015.
[16] N. Read, C. Jeffree, Low-temperature scanning electron-microscopy in biology, J. Microsc. 161 (1991) 59–72.
[17] S. Trepout, M. Sgarra, S. Marco, G. Ramm, An introduction to scanning transmission electron microscopy for the study of protozoans, Mol. Microbiol. 121 (2024) 659–670.
[18] J.Y. Kim, H. Lim, D.W. Moon, Mass spectrometry imaging of small molecules from live cells and tissues using nanomaterials, Surf. Interface Anal. 54 (2022) 381–388.
[19] A. Nyska, C.A. Cummings, A. Vainshtein, J. Nadler, N. Ezov, Y. Grunfeld, O. Gileadi, V. Behar, Electron Microscopy of wet tissues: a case study in renal pathology, Toxicol. Pathol. 32 (2004) 357–363.
[20] D.B. Peckys, G.M. Veith, D.C. Joy, N. de Jonge, Nanoscale imaging of whole cells using a liquid enclosure and a scanning transmission electron microscope, PLoS One 4 (2009) e8214.
[21] M. Salmeron, R. Schlogl, Ambient pressure photoelectron spectroscopy: a new tool for surface science and nanotechnology, Surf. Sci. Rep. 63 (2008) 169–199.
[22] C.I. Matei, C. Boulocher, C. Boule, M. Schramme, E. Viguier, T. Roger, Y. Berthier, A.M. Trunfio-Sfarghiu, M.G. Blanchin, Ultrastructural analysis of healthy synovial fluids in three mammalian species, Microsc. Microanal. 20 (2014) 903–911.
[23] T. Sakai, T. Kamiya, M. Oikawa, T. Sato, A. Tanaka, K. Ishii, JAERI Takasaki in-air micro-PIXE system for various applications, Nucl. Instrum. Methods Phys. Res. B 190 (2002) 271–275.
[24] P. Rossi, B. Doyle, V. Auzelyte, F. McDaniel, M. Mellon, Performance of an alpha-IPEM, Nucl. Instrum. Methods Phys. Res. B 249 (2006) 242–245.
[25] J. Baio, D. Graham, D. Castner, Surface analysis tools for characterizing biological materials, Chem. Soc. Rev. 49 (2020) 3278–3296.
[26] D. Castner, Biomedical surface analysis: evolution and future directions, Biointerphases 12 (2017) 02C301.
[27] A. Shchukarev, Z. Gojkovic, C. Funk, M. Ramstedt, Cryo-XPS analysis reveals surface composition of microalgae, Appl. Surf. Sci. 526 (2020) 146538.
[28] I. Schlichting, J.W. Miao, Emerging opportunities in structural biology with X-ray free-electron lasers, Curr. Opin. Struct. Biol. 22 (2012) 613–626.
[29] G. van der Schot, M. Svenda, F. Maia, M. Hantke, D.P. DePonte, M.M. Seibert, A. Aquila, J. Schulz, R. Kirian, M. Liang, F. Stellato, B. Iwan, J. Andreasson, N. Timneanu, D. Westphal, N.F. Almeida, D. Odic, D. Hasse, G.H. Carlsson, D.S. D. Larsson, A. Barty, A.V. Martin, S. Schorb, C. Bostedt, J.D. Bozek, D. Rolles, A. Rudenko, S. Epp, L. Foucar, B. Rudek, R. Hartmann, N. Kimmel, P. Holl, L. Englert, N.T.D. Loh, H.N. Chapman, I. Andersson, J. Hajdu, T. Ekeberg, Imaging single cells in a beam of live Cyanobacteria with an X-ray laser, Nat. Commun. 6 (2015) 5704.
[30] H. Ade, A.P. Hitchcock, NEXAFS microscopy and resonant scattering: composition and orientation probed in real and reciprocal space, Polymer 49 (2008) 643–675.
[31] R. Carzaniga, M.C. Domart, E. Duke, L.M. Collinson, Correlative cryo-fluorescence and cryo-soft X-Ray tomography of adherent cells at European synchrotrons, Correlative Light and Electron Microscopy Ii 124 (2014) 151–178.
[32] K.C. Dent, C. Hagen, K. Grunewald, Critical step-by-step approaches toward correlative Fluorescence/Soft X-Ray cryo-microscopy of adherent Mammalian cells, Correlative Light and Electron Microscopy Ii 124 (2014) 179–216.
[33] M. Bernhardt, J.D. Nicolas, M. Osterhoff, H. Mittelstadt, M. Reuss, B. Harke, A. Wittmeier, M. Sprung, S. Koster, T. Salditt, Correlative microscopy approach for biology using X-ray holography, X-ray scanning diffraction and STED microscopy, Nat. Commun. 9 (2018) 3641.
[34] J. Groen, J.J. Conesa, R. Valcárcel, E. Pereiro, The cellular landscape by cryo soft X-ray tomography, Biophysical Reviews 11 (2019) 611–619.
[35] I.M. Rio-Echevarria, J. Ponti, A. Bogni, D. Gilliland, M. Altissimo, L. Pascolo, G. Ceccone, A. Gianoncelli, XRF mapping and TEM analysis of coated and uncoated silica nanoparticles in A549 cells and human monocytes, X Ray Spectrom. 48 (2019) 154–161.
[36] G. Barraza-Garza, J.A. Perez-Leon, H. Castillo-Michel, L.A. de la Rosa, A. Martinez-Martinez, M. Cotte, E. Alvarez-Parrilla, Antioxidant effect of phenolic compounds (PC) at different concentrations in IEC-6 cells: a spectroscopic analysis, Spectrochim. Acta Mol. Biomol. Spectrosc. 227 (2020) 117570.
[37] M.A. Le Gros, G. McDermott, B.P. Cinquin, E.A. Smith, M. Do, W.L.L. Chao, P. P. Naulleau, C.A. Larabell, Biological soft X-ray tomography on beamline 2.1 at the Advanced light source, J. Synchrotron Radiat. 21 (2014) 1370–1377.
[38] A. Gianoncelli, C. Tufoni, M. Zizic, F. Zingaro, G. Ceccone, V. Bonanni, M. Salomé, E. Villalobos-Portillo, R. La Spina, D. Cassano, G. Ricci, P. Lorella, Ovarian cell accumulation of model PVC nanoplastics labelled with CdSe-QDs investigated by X-Ray fluorescence microscopy, X Ray Spectrom. 54 (2025) 310–321.
[39] P. Gueriau, S. Bernard, L. Bertrand, Advanced synchrotron characterization of paleontological specimens, Elements 12 (2016) 45–50.
[40] M. Voltolini, A. Haboub, S. Dou, T.H. Kwon, A.A. MacDowell, D.Y. Parkinson, J. Ajo-Franklin, The emerging role of 4D synchrotron X-ray micro-tomography for climate and fossil energy studies: five experiments showing the present capabilities at beamline 8.3.2 at the advanced light source, J. Synchrotron Radiat. 24 (2017) 1237–1249.
[41] M.D. Fonseca, B.H.S. Araujo, C.S.B. Dias, N.L. Archilha, D.P.A. Neto, E. Cavalheiro, H. Westfahl, A.J.R. da Silva, K.G. Franchini, High-resolution synchrotron-based X-ray microtomography as a tool to unveil the three-dimensional neuronal architecture of the brain, Sci. Rep. 8 (2018) 12074.
[42] C.C. Dupont-Gillain, Understanding and controlling type I collagen adsorption and assembly at interfaces, and application to cell engineering, Colloids Surf. B Biointerfaces 124 (2014) 87–96.
[43] A.M. Pinto, I.C. Goncalves, F.D. Magalhaes, Graphene-based materials biocompatibility: a review, Colloids Surf. B Biointerfaces 111 (2013) 188–202.
[44] K. Dave, V.G. Gomes, Interactions at scaffold interfaces: effect of surface chemistry, structural attributes and bioaffinity, Mater. Sci. Eng., C 105 (2019) 110078.
[45] A. Pupovac, B. Senturk, C. Griffoni, K. Maniura-Weber, M. Rottmar, S. L. McArthur, Toward immunocompetent 3D skin models, Adv. Healthcare Mater. 7 (2018) 1701405.
[46] F. Hook, B. Kasemo, The QCM-D technique for probing biomacromolecular recognition reactions, Piezoelectric Sensors 5 (2007) 425–447.
[47] E. Mauriz, M.C. Garcia-Fernandez, L.M. Lechuga, Towards the design of universal immunosurfaces for SPR-based assays: a review, TrAC, Trends Anal. Chem. 79 (2016) 191–198.
[48] S. Hosseinpour, S.J. Roeters, M. Bonn, W. Peukert, S. Woutersen, T. Weidner, Structure and dynamics of interfacial peptides and proteins from vibrational sum-frequency generation spectroscopy, Chem. Rev. 120 (2020) 3420–3465.
[49] E.B. Bahadir, M.K. Sezginturk, Applications of electrochemical immunosensors for early clinical diagnostics, Talanta 132 (2015) 162–174.

[50] S.L. McArthur, G. Mishra, C.D. Easton, Applications of XPS in biology and biointerface analysis, in: V.S. Smentkowski (Ed.), Surface Analysis and Techniques in Biology, Springer International Publishing, 2014.
[51] B.D. Ratner, S.J. Bryant, Biomaterials: where we have been and where we are going, Annu. Rev. Biomed. Eng. 6 (2004) 41–75.
[52] F. Garbassi, M. Morra, O. E., Polymer Surfaecs: from Physics to Technology, John wiley & sons, 1998.
[53] K.S. Siow, L. Britcher, S. Kumar, H.J. Griesser, Plasma methods for the generation of chemically reactive surfaces for biomolecule immobilization and cell colonization - a review, Plasma Process. Polym. 3 (2006) 392–418.
[54] E. Sardella, R. Gristina, G.S. Senesi, R. d'Agostino, P. Favia, Homogeneous and micro-patterned plasma-deposited PEO-like coatings for biomedical surfaces, Plasma Process. Polym. 1 (2004) 63–72.
[55] D. Falconnet, G. Csucs, H.M. Grandin, M. Textor, Surface engineering approaches to micropattern surfaces for cell-based assays, Biomaterials 27 (2006) 3044–3063.
[56] S.G. Zhang, L. Yan, M. Altman, M. Lassle, H. Nugent, F. Frankel, D. A. Lauffenburger, G.M. Whitesides, A. Rich, Biological surface engineering: a simple system for cell pattern formation, Biomaterials 20 (1999) 1213–1220.
[57] R. Ogaki, M. Alexander, P. Kingshott, Chemical patterning in biointerface science, Mater. Today 13 (2010) 22–35.
[58] J. Robertus, W.R. Browne, B.L. Feringa, Dynamic control over cell adhesive properties using molecular-based surface engineering strategies, Chem. Soc. Rev. 39 (2010) 354–378.
[59] M. Dubey, K. Emoto, H. Takahashi, D.G. Castner, D.W. Grainger, Affinity-Based protein surface pattern Formation by ligand self-selection from mixed protein solutions, Adv. Funct. Mater. 19 (2009) 3046–3055.
[60] P. Kingshott, G. Andersson, S.L. McArthur, H.J. Griesser, Surface modification and chemical surface analysis of biomaterials, Curr. Opin. Chem. Biol. 15 (2011) 667–676.
[61] J. Tan, H. Shen, W.M. Saltzman, Micron-scale positioning of features influences the rate of polymorphonuclear leukocyte migration, Biophys. J. 81 (2001) 2569–2579.
[62] Y. Yokoyama, S. Aoyagi, M. Fujii, J. Matsuo, J.S. Fletcher, N.P. Lockyer, J. C. Vickerman, M.K. Passarelli, R. Havelund, M.P. Seah, Peptide fragmentation and surface structural analysis by means of ToF-SIMS using large cluster ion sources, Anal. Chem. 88 (2016) 3592–3597.
[63] H. Fabre, D. Mercier, A. Galtayries, D. Portet, N. Delorme, J.F. Bardeau, Impact of hydrophilic and hydrophobic functionalization of flat TiO2/Ti surfaces on proteins adsorption, Appl. Surf. Sci. 432 (2018) 15–21.
[64] U. Czuba, R. Quintana, P. Lassaux, R. Bombera, G. Ceccone, J. Banuls-Ciscar, M. Moreno-Couranjou, C. Detrembleur, P. Choquet, Anti-biofouling activity of Ranaspumin-2 bio-surfactant immobilized on catechol-functional PMMA thin layers prepared by atmospheric plasma deposition, Colloids Surf. B Biointerfaces 178 (2019) 120–128.
[65] V. Spampinato, G. Ceccone, S. Giordani, Surface analysis of zinc-porphyrin functionalized carbon nano-onions, Biointerphases 10 (2015) 019006.
[66] F. Fumagalli, A. Welle, G. Bucher, S. Appleton, J. Ponti, G. Ceccone, L. Calzolai, D. Mehn, Secondary ions mass spectrometric method for assessing surface density of pegylated liposomal nanomedicines, Sci. Rep. 15 (2025) 27060.
[67] J. Park, H. Jeong, B. Kang, S. Kim, S. Park, S. Kang, H. Kim, J. Choi, D. Hwang, T. Lee, Multi-dimensional TOF-SIMS analysis for effective profiling of disease-related ions from the tissue surface, Sci. Rep. 5 (2015) 11077.
[68] P. Agui-Gonzalez, S. Jahne, N.T.N. Phan, SIMS imaging in neurobiology and cell biology, J. Anal. At. Spectrom. 34 (2019) 1355–1368.
[69] J.S. Fletcher, Latest applications of 3D ToF-SIMS bio-imaging, Biointerphases 10 (2015) 018902.
[70] C.M. Mahoney, D.V. Patwardhan, M.K. McDermott, Characterization of drug-eluting stent (DES) materials with cluster secondary ion mass spectrometry (SIMS), Appl. Surf. Sci. 252 (2006) 6554–6557.
[71] J.C. Vickerman, N. Winograd, SIMS-A precursor and partner to contemporary mass spectrometry, Int. J. Mass Spectrom. 377 (2015) 568–579.
[72] M. Kompauer, S. Heiles, B. Spengler, Atmospheric pressure MALDI mass spectrometry imaging of tissues and cells at 1.4-mu m lateral resolution, Nat. Methods 14 (2017) 90–96.
[73] M.K. Passarelli, A. Pirkl, R. Moellers, D. Grinfeld, F. Kollmer, R. Havelund, C. F. Newman, P.S. Marshall, H. Arlinghaus, M.R. Alexander, A. West, S. Horning, E. Niehuis, A. Makarov, C.T. Dollery, I.S. Gilmore, The 3D OrbiSIMS-label-free metabolic imaging with subcellular lateral resolution and high mass-resolving power, Nat. Methods 14 (2017) 1175.
[74] I.S. Gilmore, S. Heiles, C.L. Pieterse, Metabolic imaging at the single-cell scale: recent advances in mass spectrometry imaging, Annu. Rev. Anal. Chem. 12 (12) (2019) 201–224.
[75] J.S. Fletcher, J.C. Vickerman, N. Winograd, Label free biochemical 2D and 3D imaging using secondary ion mass spectrometry, Curr. Opin. Chem. Biol. 15 (2011) 733–740.
[76] N. Xia, C.J. May, S.L. McArthur, D.G. Castner, Time-of-flight secondary ion mass spectrometry analysis of conformational changes in adsorbed protein films, Langmuir 18 (2002) 4090–4097.
[77] S. Parry, N. Winograd, High-resolution TOF-SIMS imaging of eukaryotic cells preserved in a trehalose matrix, Anal. Chem. 77 (2005) 7950–7957.
[78] D.M. Cannon, M.L. Pacholski, N. Winograd, A.G. Ewing, Molecule specific imaging of freeze-fractured, frozen-hydrated model membrane systems using mass spectrometry, J. Am. Chem. Soc. 122 (2000) 603–610.
[79] S. Yoon, T.G. Lee, Biological tissue sample preparation for time-of-flight secondary ion mass spectrometry (ToF-SIMS) imaging, Nano Convergence 5 (2018) 24.
[80] P. Sjovall, B. Johansson, J. Lausmaa, Localization of lipids in freeze-dried mouse brain sections by imaging TOF-SIMS, Appl. Surf. Sci. 252 (2006) 6966–6974.
[81] J. Malm, D. Giannaras, M.O. Riehle, N. Gadegaard, P. Sjovall, Fixation and drying protocols for the preparation of cell samples for time-of-flight secondary ion mass spectrometry analysis, Anal. Chem. 81 (2009) 7197–7205.
[82] D. Belazi, S. Sole-Domenech, B. Johansson, M. Schalling, P. Sjovall, Chemical analysis of osmium tetroxide staining in adipose tissue using imaging ToF-SIMS, Histochem. Cell Biol. 132 (2009) 105–115.
[83] I. Lanekoff, M.E. Kurczy, R. Hill, J.S. Fletcher, J.C. Vickerman, N. Winograd, P. Sjovall, A.G. Ewing, Time of flight mass spectrometry imaging of samples fractured in situ with a spring-loaded trap system, Anal. Chem. 82 (2010) 6652–6659.
[84] J.S. Fletcher, S. Rabbani, A. Henderson, N.P. Lockyer, J.C. Vickerman, Three-dimensional mass spectral imaging of HeLa-M cells - sample preparation, data interpretation and visualisation, Rapid Commun. Mass Spectrom. 25 (2011) 925–932.
[85] K. Schaepe, J. Kokesch-Himmelreich, M. Rohnke, A.S. Wagner, T. Schaaf, A. Henss, S. Wenisch, J. Janek, Storage of cell samples for ToF-SIMS experiments-how to maintain sample integrity, Biointerphases 11 (2016) 02A313.
[86] K. Schaepe, J. Kokesch-Himmelreich, M. Rohnke, A.S. Wagner, T. Schaaf, S. Wenisch, J. Janek, Assessment of different sample preparation routes for mass spectrometric monitoring and imaging of lipids in bone cells via ToF-SIMS, Biointerphases 10 (2015) 019016.
[87] S. Van Nuffel, C. Parmenter, D.J. Scurr, N.A. Russell, M. Zelzer, Multivariate analysis of 3D ToF-SIMS images: method validation and application to cultured neuronal networks, Analyst 141 (2016) 90–95.
[88] L.H.S. Jensen, T. Cheng, F.O.V. Plane, S. Escrig, A. Comment, B. van den Brandt, B.M. Humbel, A. Meibom, En route to ion microprobe analysis of soluble compounds at the single cell level: the CryoNanoSIMS. European Microscopy Congress, 2016, p. 455.
[89] K. Kuroda, T. Fujiwara, T. Imai, R. Takama, K. Saito, Y. Matsushita, K. Fukushima, The cryo-TOF-SIMS/SEM system for the analysis of the chemical distribution in freeze-fixed Cryptomeria japonica wood, Surf. Interface Anal. 45 (2013) 215–219.
[90] K.L. McDonald, M. Auer, High-pressure freezing, cellular tomography, and structural cell biology, Biotechniques 41 (2006) 137. +.
[91] N. Winograd, A. Bloom, Sample preparation for 3D SIMS chemical imaging of cells, mass spectrometry imaging of small, Molecules 1203 (2015) 9–19.
[92] H. Nygren, K. Borner, P. Malmberg, E. Tallarek, B. Hagenhoff, Imaging TOF-SIMS of rat kidney prepared by high-pressure freezing, Microsc. Res. Tech. 68 (2005) 329–334.
[93] R. Dahl, L.A. Staehelin, High-pressure freezing for the preservation of biological structure - theory and practice, J. Electron. Microsc. Tech. 13 (1989) 165–174.
[94] A. Körber, I.G.M. Anthony, R.M.A. Heeren, Mass spectrometry imaging, Anal. Chem. 97 (2025) 15517–15549.
[95] A. Valsesia, M.M. Silvan, G. Ceccone, D. Gilliland, P. Colpo, F.O. Rossi, Acid/base micropatterned devices for pH-dependent biosensors, Plasma Process. Polym. 2 (2005) 334–339.
[96] P.J. Rivero, A. Urrutia, J. Goicoechea, F.J. Arregui, Nanomaterials for functional textiles and fibers, Nanoscale Res. Lett. 10 (2015) 22.
[97] M.N. Macgregor, A. Michelmore, H.S. Shirazi, J. Whittle, K. Vasilev, Secrets of plasma-deposited polyoxazoline functionality lie in the plasma phase, Chem. Mater. 29 (2017) 8047–8051.
[98] A. Vesel, J. Kovac, G. Primc, I. Junkar, M. Mozetic, Effect of H2S plasma treatment on the surface modification of a polyethylene terephthalate surface, Materials 9 (2016) 95.
[99] A. Henderson, Multivariate analysis of SIMS spectra, in: JC, D.B. Vickermann (Eds.), TOF-SIMS: Materials Analysis by Mass Spectrometry, 2013, p. 449.
[100] S. Chatterjee, B. Singh, A. Diwan, Z.R. Lee, M.H. Engelhard, J. Terry, H.D. Tolley, N.B. Gallagher, M.R. Linford, A perspective on two chemometrics tools: PCA and MCR, and introduction of a new one: pattern recognition entropy (PRE), as applied to XPS and ToF-SIMS depth profiles of organic and inorganic materials, Appl. Surf. Sci. 433 (2018) 994–1017.
[101] G.F. Trindade, M.L. Abel, C. Lowe, R. Tshulu, J.F. Watts, A time-of-flight secondary ion Mass spectrometry/Multivariate analysis (ToF-SIMS/MVA) approach to identify phase segregation in blends of incompatible but extremely similar resins, Anal. Chem. 90 (2018) 3936–3941.
[102] R.M.T. Madiona, N.G. Welch, B.W. Muir, D.A. Winkler, P.J. Pigram, Rapid evaluation of immobilized immunoglobulins using automated mass-segmented ToF-SIMS, Biointerphases 14 (2019) 061002.
[103] M.S. Wagner, D.G. Castner, Characterization of adsorbed protein films by time-of-flight secondary ion mass spectrometry with principal component analysis, Langmuir 17 (2001) 4649–4660.
[104] S. Aoyagi, Y. Fujiwara, A. Takano, J. Vorng, I. Gilmore, Y. Wang, E. Tallarek, B. Hagenhoff, S. Iida, A. Luch, H. Jungnickel, Y. Lang, H. Shon, T. Lee, Z. Li, K. Matsuda, I. Mihara, A. Miisho, Y. Murayama, T. Nagatomi, R. Ikeda, M. Okamoto, K. Saiga, T. Tsuchiya, S. Uemura, Evaluation of time-of-flight secondary ion mass spectrometry spectra of peptides by random forest with amino acid labels: results from a versailles project on advanced materials and standards interlaboratory study, Anal. Chem. 93 (2021) 4191–4197.
[105] L.M. Gordon, L. Tran, D. Joester, Atom probe tomography of apatites and bone-type mineralized tissues, ACS Nano 6 (2012) 10667–10675.

[106] D.E. Perea, J. Liu, J. Bartrand, Q. Dicken, S.T. Thevuthasan, N.D. Browning, J. E. Evans, Atom probe tomographic mapping directly reveals the atomic distribution of phosphorus in resin embedded ferritin, Sci. Rep. 6 (2016) 22321.
[107] K. Narayan, T.J. Prosa, J. Fu, T.F. Kelly, S. Subramaniam, Chemical mapping of mammalian cells by atom probe tomography, J. Struct. Biol. 178 (2012) 98–107.
[108] E. van Duijn, Current limitations in native mass spectrometry based structural biology, J. Am. Soc. Mass Spectrom. 21 (2010) 971–978.
[109] R. Aebersold, M. Mann, Mass spectrometry-based proteomics, Nature 422 (2003) 198–207.
[110] Y.T. Yang, C. Callegari, X.L. Feng, K.L. Ekinci, M.L. Roukes, Zeptogram-Scale nanomechanical mass sensing, Nano Lett. 6 (2006) 583–586.
[111] J. Tamayo, P.M. Kosaka, J.J. Ruz, A. San Paulo, M. Calleja, Biosensors based on nanomechanical systems, Chem. Soc. Rev. 42 (2013) 1287–1311.
[112] K.L. Ekinci, M.L. Roukes, Nanoelectromechanical systems, Rev. Sci. Instrum. 76 (2005) 061101.
[113] B. Anja, D. Søren, K. Stephan Sylvest, S. Silvan, T. Maria, Cantilever-like micromechanical sensors, Rep. Prog. Phys. 74 (2011) 036101.
[114] J.J. Ruz, O. Malvar, E. Gil-Santos, D. Ramos, M. Calleja, J. Tamayo, A review on theory and modelling of nanomechanical sensors for biological applications, Processes 9 (2021) 164.
[115] J. Tamayo, P. Kosaka, J. Ruz, A. San Paulo, M. Calleja, Biosensors based on nanomechanical systems, Chem. Soc. Rev. 42 (2013) 1287–1311.
[116] T.P. Burg, M. Godin, S.M. Knudsen, W. Shen, G. Carlson, J.S. Foster, K. Babcock, S.R. Manalis, Weighing of biomolecules, single cells and single nanoparticles in fluid, Nature 446 (2007) 1066–1069.
[117] T.P. Burg, S.R. Manalis, Suspended microchannel resonators for biomolecular detection, Appl. Phys. Lett. 83 (2003) 2698.
[118] W.H. Grover, A.K. Bryan, M. Diez-Silva, S. Suresh, J.M. Higgins, S.R. Manalis, Measuring single-cell density, Proc. Natl. Acad. Sci. 108 (2011) 10992–10996.
[119] A.K. Naik, M.S. Hanay, W.K. Hiebert, X.L. Feng, M.L. Roukes, Towards single-molecule nanomechanical mass spectrometry, Nat. Nanotechnol. 4 (2009) 445–450.
[120] M.S. Hanay, S. Kelber, A.K. Naik, D. Chi, S. Hentz, E.C. Bullard, E. Colinet, L. Duraffourg, M.L. Roukes, Single-protein nanomechanical mass spectrometry in real time, Nat. Nanotechnol. 7 (2012) 602–608.
[121] O. Malvar, J. Ruz, P. Kosaka, C. Domínguez, E. Gil-Santos, M. Calleja, J. Tamayo, Mass and stiffness spectrometry of nanoparticles and whole intact bacteria by multimode nanomechanical resonators, Nat. Commun. 7 (2016) 13452.
[122] M.S. Hanay, S.I. Kelber, C.D. O'Connell, P. Mulvaney, J.E. Sader, M.L. Roukes, Inertial imaging with nanomechanical systems, Nat Nano 10 (2015) 339–344.
[123] E. Sage, A. Brenac, T. Alava, R. Morel, C. Dupré, M.S. Hanay, M.L. Roukes, L. Duraffourg, C. Masselon, S. Hentz, Neutral particle mass spectrometry with nanomechanical systems, Nat. Commun. 6 (2015) 6482.
[124] A. Sanz-Jiménez, O. Malvar, J. Ruz, S. García-López, P. Kosaka, E. Gil-Santos, A. Cano, D. Papanastasiou, D. Kounadis, J. Mingorance, A. Paulo, M. Calleja, J. Tamayo, High-throughput determination of dry mass of single bacterial cells by ultrathin membrane resonators, Commun. Biol. 5 (2022) 1227.
[125] S. Dominguez-Medina, S. Fostner, M. Defoort, M. Sansa, A.-K. Stark, M.A. Halim, E. Vernhes, M. Gely, G. Jourdan, T. Alava, P. Boulanger, C. Masselon, S. Hentz, Neutral mass spectrometry of virus capsids above 100 megadaltons with nanomechanical resonators, Science 362 (2018) 918–922.
[126] T. Javier, P. Valerio, K. Prisicila, F.M. Nicolas, A. Oscar, C. Montserrat, Imaging the surface stress and vibration modes of a microcantilever by laser beam deflection microscopy, Nanotechnology 23 (2012) 315501.
[127] L. Morawska, J.L.W. Tang, W. Bahnfleth, P.M. Bluyssen, A. Boerstra, G. Buonanno, J.J. Cao, S. Dancer, A. Floto, F. Franchimon, C. Haworth, J. Hogeling, C. Isaxon, J.L. Jimenez, J. Kurnitski, Y.G. Li, M. Loomans, G. Marks, L.C. Marr, L. Mazzarella, A.K. Melikov, S. Miller, D.K. Milton, W. Nazaroff, P. V. Nielsen, C. Noakes, J. Peccia, X. Querol, C. Sekhar, O. Seppanen, S. Tanabe, R. Tellier, K.W. Tham, P. Wargocki, A. Wierzbicka, M.S. Yao, How can airborne transmission of COVID-19 indoors be minimised? Environ. Int. 142 (2020) 105832.
[128] B. Ilic, Y. Yang, H.G. Craighead, Virus detection using nanoelectromechanical devices, Appl. Phys. Lett. 85 (2004) 2604–2606.
[129] E. Gil-Santos, J.J. Ruz, O. Malvar, I. Favero, A. Lemaitre, P.M. Kosaka, S. Garcia-Lopez, M. Calleja, J. Tamayo, Optomechanical detection of vibration modes of a single bacterium, Nat. Nanotechnol. 15 (2020) 469. +.
[130] R.T. Erdogan, M. Alkhaled, B.E. Kaynak, H. Alhmoud, H.S. Pisheh, M. Kelleci, I. Karakurt, C. Yanik, Z.B. Sen, B. Sari, A.M. Yagci, A. Ozkul, M.S. Hanay, Atmospheric pressure mass spectrometry of single viruses and nanoparticles by nanoelectromechanical systems, ACS Nano 16 (2022) 3821–3833.
[131] O. Malvar, E. Gil-Santos, J. Ruz, E. Sentre-Arribas, A. Sanz-Jimenez, P. Kosaka, S. Garcia-Lopez, A. Paulo, S. Sbarra, L. Waquier, I. Favero, M. van der Heiden, R. Altmann, D. Papanastasiou, D. Kounadis, I. Panagiotopoulos, J. Mingorance, M. Rodríguez-Tejedor, R. Delgado, M. Calleja, J. Tamayo, Multifrequency nanomechanical mass spectrometer prototype for measuring viral particles using optomechanical disk resonators, IEEE, MEMS 36 (2023) 153–156.
[132] Z. Mi, C. Chen, H. Tan, Y. Dou, C. Yang, S. Turaga, M. Ren, S. Vajandar, G. Yuen, T. Osipowicz, F. Watt, A. Bettiol, Quantifying nanodiamonds biodistribution in whole cells with correlative iono-nanoscopy, Nat. Commun. 12 (2021) 4657.
[133] C. Udalagama, A.A. Bettiol, F. Watt, Stochastic spatial energy deposition profiles for MeV protons and keV electrons, Phys. Rev. B 80 (2009) 224107.
[134] A.A. Bettiol, Z.H. Mi, F. Watt, High-resolution fast ion microscopy of single whole biological cells, Appl. Phys. Rev. 3 (2016) 041102.
[135] S.J. Mulware, The review of nuclear microscopy techniques: an approach for nondestructive trace elemental analysis and mapping of biological materials, J. Biophys. 2015 (2015) 740751.
[136] B. Jencic, P. Vavpetic, M. Kelemen, M. Vencelj, K. Vogel-Mikus, A. Kavcic, P. Pelicon, MeV-SIMS TOF imaging of organic tissue with continuous primary beam, J. Am. Soc. Mass Spectrom. 30 (2019) 1801–1812.
[137] J. Becker, U. Breuer, H. Hsieh, T. Osterholt, U. Kumtabtim, B. Wu, A. Matusch, J. Caruso, Z. Qin, Bioimaging of metals and biomolecules in mouse heart by laser ablation inductively coupled plasma mass spectrometry and secondary ion mass spectrometry, Anal. Chem. 82 (2010) 9528–9533.
[138] J. de Jesus, C. Costa, A. Burton, V. Palitsin, R. Webb, A. Taylor, C. Nikula, A. Dexter, F. Kaya, M. Chambers, V. Dartois, R. Goodwin, J. Bunch, M. Bailey, Correlative imaging of trace elements and intact molecular species in a single-tissue sample at the 50 μm scale, Anal. Chem. 93 (2021) 13450–13458.
[139] https://nucleus.iaea.org/sites/accelerators/Pages/beamtime.aspx. https://www.ionbeamcenters.eu/radiate/radiate-transnational-access/.
[140] I. Jaric, M. Lenhardt, J. Pallon, M. Elfman, A. Kalauzi, R. Suciu, G. Cvijanovic, T. Ebenhard, Insight into danube sturgeon life history: trace element assessment in pectoral fin rays, Environ. Biol. Fish. 90 (2011) 171–181.
[141] R.M. Godinho, M.T. Cabrita, L.C. Alves, T. Pinheiro, Imaging of intracellular metal partitioning in marine diatoms exposed to metal pollution: consequences to cellular toxicity and metal fate in the environment, Metallomics 6 (2014) 1626–1631.
[142] M. Ugarte, N.N. Osborne, L.A. Brown, P.N. Bishop, Iron, zinc, and copper in retinal physiology and disease, Surv. Ophthalmol. 58 (2013) 585–609.
[143] R. Rajendran, M.Q. Ren, M.D. Ynsa, G. Casadesus, M.A. Smith, G. Perry, B. Halliwell, F. Watt, A novel approach to the identification and quantitative elemental analysis of amyloid deposits-insights into the pathology of alzheimer's disease, Biochem. Biophys. Res. Commun. 382 (2009) 91–95.
[144] H. Ren Minqin, Reshmi Rajendran, Ning Pan, Benny and Wei-Yi ong and frank Watt and Barry, the iron chelator desferrioxamine inhibits atherosclerotic lesion development and decreases lesion iron concentrations in the cholesterol-fed rabbit, Free Radic. Biol. Med. 38 (2005) 1206–1211.
[145] M.D. Ynsa, M.Q. Ren, R. Rajendran, J.N. Sidhapuriwala, J.A. van Kan, M. Bhatia, F. Watt, Zinc mapping and density imaging of rabbit pancreas endocrine tissue sections using nuclear microscopy, Microsc. Microanal. 15 (2009) 345–352.
[146] A. van der Ent, W.J. Przybylowicz, M.D. de Jonge, H.H. Harris, C.G. Ryan, G. Tylko, D.J. Paterson, A.D. Barnabas, P.M. Kopittke, J. Mesjasz-Przybylowicz, X-ray elemental mapping techniques for elucidating the ecophysiology of hyperaccumulator plants, New Phytol. 218 (2018) 432–452.
[147] T. Pinheiro, J. Pallon, L.C. Alves, A. Verissimo, P. Filipe, J.N. Silva, R. Silva, The influence of corneocyte structure on the interpretation of permeation profiles of nanoparticles across skin, Nucl. Instrum. Methods Phys. Res. Sect. B Beam Interact. Mater. Atoms 260 (2007) 119–123.
[148] L. Perrin, A. Carmona, S. Roudeau, R. Ortega, Evaluation of sample preparation methods for single cell quantitative elemental imaging using proton or synchrotron radiation focused beams, J. Anal. At. Spectrom. 30 (2015) 2525–2532.
[149] Z. Siketic, I.B. Radovic, M. Jaksic, M.P. Hadzija, M. Hadzija, Submicron mass spectrometry imaging of single cells by combined use of mega electron volt time-of-flight secondary ion mass spectrometry and scanning transmission ion microscopy, Appl. Phys. Lett. 107 (2015) 093702.
[150] B. Jencic, L. Jeromel, N.O. Potocnik, K. Vogel-Mikus, E. Kovacec, M. Regvar, Z. Siketic, P. Vavpetic, Z. Rupnik, K. Bucar, M. Kelemen, J. Kovac, P. Pelicon, Molecular imaging of cannabis leaf tissue with MeV-SIMS method, Nucl. Instrum. Methods Phys. Res. Sect. B Beam Interact. Mater. Atoms 371 (2016) 205–210.
[151] X. Chen, C.B. Chen, C.N.B. Udalagama, M.Q. Ren, K.E. Fong, L.Y.L. Yung, P. Giorgia, A.A. Bettiol, F. Watt, High-Resolution 3D imaging and quantification of gold nanoparticles in a whole cell using scanning transmission ion microscopy, Biophys. J. 104 (2013) 1419–1425.
[152] M.S. Vasco, L.C. Alves, V. Corregidor, D. Correia, C.P. Godinho, I. Sa-Correia, A. Bettiol, F. Watt, T. Pinheiro, 3D map distribution of metallic nanoparticles in whole cells using MeV ion microscopy, J. Microsc. 267 (2017) 227–236.
[153] C. Michelet, Z.X. Li, W. Yang, S. Incerti, P. Desbarats, J.F. Giovannelli, P. Barberet, M.H. Delville, N. Gordillo, G. Deves, H. Seznec, A Geant4 simulation for three-dimensional proton imaging of microscopic samples, Physica Medica-European Journal of Medical Physics 65 (2019) 172–180.
[154] P. Filipe, J.N. Silva, R. Silva, J.L.C. de Castro, M.M. Gomes, L.C. Alves, R. Santus, T. Pinheiro, Stratum Corneum is an effective barrier to TiO2 and ZnO nanoparticle percutaneous absorption, Skin Pharmacol. Physiol. 22 (2009) 266–275.
[155] B. Gulson, M.J. McCall, D.M. Bowman, T. Pinheiro, A review of critical factors for assessing the dermal absorption of metal oxide nanoparticles from sunscreens applied to humans, and a research strategy to address current deficiencies, Arch. Toxicol. 89 (2015) 1909–1930.
[156] M. Simon, G. Saez, G. Muggiolu, M. Lavenas, Q. Le Trequesser, C. Michelet, G. Deves, P. Barberet, E. Chevet, D. Dupuy, M.H. Delville, H. Seznec, In situ quantification of diverse titanium dioxide nanoparticles unveils selective endoplasmic reticulum stress-dependent toxicity, Nanotoxicology 11 (2017) 134–145.
[157] P. Sa-Pereira, M.S. Diniz, L. Moita, T. Pinheiro, E. Mendonca, S.M. Paixao, A. Picado, Protein profiling as early detection biomarkers for TiO2 nanoparticle toxicity in Daphnia magna, Ecotoxicology 27 (2018) 430–439.
[158] O. Lozano, J.L. Colaux, J. Laloy, L. Alpan, J.M. Dogne, S. Lucas, Fast, asymmetric and nonhomogeneous clearance of SiC nanoaerosol assessed by micro-particle-induced x-ray emission, Nanomedicine 13 (2018) 145–155.

[159] T. Pinheiro, L. Alves, A. Matos, I. Correia, J. Pessoa, F. Marques, Cellular targets of cytotoxic copper phenanthroline complexes: a multimodal imaging quantitative approach in single PC3 cells, Metallomics 16 (2024) mfae051.
[160] B. Dominelli, C. Jakob, J. Oberkofler, P. Fischer, E. Esslinger, R. Reich, F. Marques, T. Pinheiro, J. Correia, F. Kühn, Mechanisms underlying the cytotoxic activity of syn/anti-isomers of dinuclear Au(I) NHC complexes, Eur. J. Med. Chem. 203 (2020) 112576.
[161] C. Habchi, D.T. Nguyen, G. Deves, S. Incerti, L. Lernelle, P.L. Van Vang, P. Moretto, R. Ortega, H. Seznec, A. Sakellariou, C. Sergeant, A. Simionovici, M. D. Ynsa, E. Gontier, M. Heiss, T. Pouthier, A. BoudoU, F. Rebillat, Three-dimensional densitometry imaging of diatom cells using STIM tomography, Nucl. Instrum. Methods Phys. Res. Sect. B Beam Interact. Mater. Atoms 249 (2006) 653–659.
[162] T. Andrea, M. Rothermel, R. Werner, T. Butz, T. Reinert, Limited angle STIM and PIXE tomography of single cells, Nucl. Instrum. Methods Phys. Res. Sect. B Beam Interact. Mater. Atoms 268 (2010) 1884–1888.
[163] D.G. Beasley, L.C. Alves, P. Barberet, S. Bourret, G. Deves, N. Gordillo, C. Michelet, Q. Le Trequesser, A.C. Marques, H. Seznec, R.C. da Silva, A comparison of quantitative reconstruction techniques for PIXE-tomography analysis applied to biological samples, Nucl. Instrum. Methods Phys. Res. Sect. B Beam Interact. Mater. Atoms 331 (2014) 248–252.
[164] R. Johnson, An Introduction to Environmental Scanning Electron Microscopy, Philips Electron Optics, Eindhoven, The Netherlands, 1996.
[165] R. Toyoshima, H. Kondoh, In-situ observations of catalytic surface reactions with soft x-rays under working conditions, J. Phys. Condens. Matter 27 (2015) 083003.
[166] A.K. Pathan, J. Bond, R.E. Gaskin, Sample preparation for SEM of plant surfaces, Mater. Today 12 (2010) 32–43.
[167] Y.L. Ren, A.M. Donald, Z.B. Zhang, Investigation of the morphology, viability and mechanical properties of yeast cells in environmental SEM, Scanning 30 (2008) 435–442.
[168] J.A. Callow, M.P. Osborne, M.E. Callow, F. Baker, A.M. Donald, Use of environmental scanning electron microscopy to image the spore adhesive of the marine alga Enteromorpha in its natural hydrated state, Colloids Surf. B Biointerfaces 27 (2003) 315–321.
[169] J.E. McGregor, A.M. Donald, ESEM imaging of dynamic biological processes: the closure of stomatal pores, J. Microsc. 239 (2010) 135–141.
[170] D.J. Stokes, S.M. Rea, S.M. Best, W. Bonfield, Electron microscopy of mammalian cells in the absence of fixing, freezing, dehydration, or specimen coating, Scanning 25 (2003) 181–184.
[171] M.G. Gandolfi, G. Iezzi, A. Piattelli, C. Prati, A. Scarano, Osteoinductive potential and bone-bonding ability of ProRoot MTA, MTA plus and Biodentine in rabbit intramedullary model: microchemical characterization and histological analysis, Dent. Mater. 33 (2017) E221–E238.
[172] Y.H. Zhu, C.Z. Li, Effect of doped silicon on structure and magnetic properties of gamma-Fe2O3 particles, Mater. Chem. Phys. 51 (1997) 169–173.
[173] N.M. Thomson, K. Channon, N.A. Mokhtar, L. Staniewicz, R. Rai, I. Roy, S. Sato, T. Tsuge, A.M. Donald, D. Summers, E. Sivaniah, Imaging internal features of whole, unfixed bacteria, Scanning 33 (2011) 59–68.
[174] J.M. Alonso, T. Ondarcuhu, C. Parrens, M. Gorzny, A.M. Bittner, Nanoscale wetting of viruses by ionic liquids, J. Mol. Liq. 276 (2019) 667–674.
[175] T.U. Nisa, S.M. Kamranullah, A. Tahir, H. Ahmed, W. Abbas, M. Iqbal, S. Khan, In vitro evaluation of antiviral activity of Sisybrium irio (Khaksi) against SARS-COV-2, Pak. J. Pharm. Sci. 35 (2022) 859–864.
[176] D.B. Peckys, U. Korf, N. de Jonge, Local variations of HER2 dimerization in breast cancer cells discovered by correlative fluorescence and liquid electron microscopy, Sci, Adv 1 (2015) e1500165.
[177] C. Rodriguez, Torres-Costa, A. Bittner, S. Morin, M. Castresana, S. Chiriaev, E. Modin, A. Chuvilin, M. Silván, Electron microscopy approach to the wetting dynamics of single organosilanized mesopores, iScience 26 (2023) 107981.
[178] G. Olivieri, J.B. Giorgi, R.G. Green, M.A. Brown, 5 years of ambient pressure photoelectron spectroscopy (APPES) at the Swiss Light source (SLS), J. Electron. Spectrosc. Relat. Phenom. 216 (2017) 1–16.
[179] P.M. Dietrich, S. Bahr, T. Yamamoto, M. Meyer, A. Thissen, Chemical surface analysis on materials and devices under functional conditions - environmental photoelectron spectroscopy as non-destructive tool for routine characterization, J. Electron. Spectrosc. Relat. Phenom. 231 (2019) 118–126.
[180] M. Kjaervik, K. Schwibbert, P. Dietrich, A. Thissen, W.E.S. Unger, Surface characterisation of Escherichia coli under various conditions by near-ambient pressure XPS, Surf. Interface Anal. 50 (2018) 996–1000.
[181] D. Shah, T. Roychowdhury, S. Bahr, P. Dietrich, M. Meyer, A. Thissen, M. R. Linford, Human tooth, by near-ambient pressure x-ray photoelectron spectroscopy, Surf. Sci. Spectra 26 (2019) 014016.
[182] C. Rodriguez, P. Dietrich, V. Torres-Costa, V. Cebrian, C. Gomez-Abad, A. Diaz, O. Ahumada, M.M. Silvan, Near ambient pressure X-ray photoelectron spectroscopy monitoring of the surface immobilization cascade on a porous silicon-gold nanoparticle FET biosensor, Appl. Surf. Sci. 492 (2019) 362–368.
[183] F.J. Fernández-Alonso, R. Calvo, A. Sanz, I.J. Villar-García, F. Saiz, M. Hernando-Pérez, V.P. Dieste, M.M. Silván, Water partial pressure X-ray photoelectron spectroscopy study of the conformation of fibrinogen on silanized hydrophilic/hydrophobic surfaces, Surf. Interfaces 72 (2025) 106964.
[184] J.J. Velasco-Velez, V. Pfeifer, M. Havecker, R.S. Weatherup, R. Arrigo, C. H. Chuang, E. Stotz, G. Weinberg, M. Salmeron, R. Schlogl, A. Knop-Gericke, Photoelectron spectroscopy at the graphene-liquid interface reveals the electronic structure of an electrodeposited Cobalt/Graphene electrocatalyst, Angew. Chem., Int. Ed. 54 (2015) 14554–14558.
[185] A. Kolmakov, D.A. Dikin, L.J. Cote, J.X. Huang, M.K. Abyaneh, M. Amati, L. Gregoratti, S. Gunther, M. Kiskinova, Graphene oxide windows for in situ environmental cell photoelectron spectroscopy, Nat. Nanotechnol. 6 (2011) 651–657.
[186] S. Thiberge, A. Nechushtan, D. Sprinzak, O. Gileadi, V. Behar, O. Zik, Y. Chowers, S. Michaeli, J. Schlessinger, E. Moses, Scanning electron microscopy of cells and tissues under fully hydrated conditions, Proc. Natl. Acad. Sci. U. S. A 101 (2004) 3346–3351.
[187] T. Prozorov, T.P. Almeida, A. Kovacs, R.E. Dunin-Borkowski, Off-axis electron holography of bacterial cells and magnetic nanoparticles in liquid, J. R. Soc., Interface 14 (2017) 20170464.
[188] S. Besztejan, S. Keskin, S. Manz, G. Kassier, R. Bucker, D. Venegas-Rojas, H. K. Trieu, A. Rentmeister, R.J.D. Miller, Visualization of cellular components in a Mammalian cell with liquid-cell transmission electron microscopy, Microsc. Microanal. 23 (2017) 46–55.
[189] Q. Chen, J.M. Smith, J. Park, K. Kim, D. Ho, H.I. Rasool, A. Zettl, A.P. Alivisatos, 3D motion of DNA-Au nanoconjugates in graphene Liquid Cell Electron Microscopy, Nano Lett. 13 (2013) 4556–4561.
[190] X. Hua, C. Szymanski, Z.Y. Wang, Y.F. Zhou, X. Ma, J.C. Yu, J. Evans, G. Orr, S. Q. Liu, Z.H. Zhu, X.Y. Yu, Chemical imaging of molecular changes in a hydrated single cell by dynamic secondary ion mass spectrometry and super-resolution microscopy, Integr. Biol. 8 (2016) 635–644.
[191] J.M. Yuk, J. Park, P. Ercius, K. Kim, D.J. Hellebusch, M.F. Crommie, J.Y. Lee, A. Zettl, A.P. Alivisatos, High-Resolution EM of colloidal nanocrystal growth using graphene liquid cells, Science 336 (2012) 61–64.
[192] R.M.A. Heeren, Molecular cellophane, Nat. Methods 18 (2021) 242–243.
[193] Y.Y. Liu, Y.L. Ying, X. Hua, Y.T. Long, In-situ discrimination of the water cluster size distribution in aqueous solution by ToF-SIMS, Sci. China Chem. 61 (2018) 159–163.
[194] P. Vavpetic, K. Vogel-Mikus, L. Jeromel, N.O. Potocnik, P. Pongrac, D. Drobne, Z. P. Tkalec, S. Novak, M. Kos, S. Koren, M. Regvar, P. Pelicon, Elemental distribution and sample integrity comparison of freeze-dried and frozen-hydrated biological tissue samples with nuclear microprobe, Nucl. Instrum. Methods Phys. Res. Sect. B Beam Interact. Mater. Atoms 348 (2015) 147–151.
[195] G. Tylko, J. Mesjasz-Przybylowicz, W.J. Przybylowicz, In-vacuum micro-PIXE analysis of biological specimens in frozen-hydrated state, Nucl. Instrum. Methods Phys. Res. Sect. B Beam Interact. Mater. Atoms 260 (2007) 141–148.